Article

Single-cell RNA sequencing identifies hippocampal microglial dysregulation in diet-induced obesity

No morphological differences in hippocampal microglia

Adolescent mice

Ctrl **HFD**

Single-cell RNA-seq analysis of hippocampal microglia

1 mo HFD → 3 mo HFD →

Early signature of dysregulation of ER homeostasis **Later signature of inflammatory response**

Rosemary E. Henn, Kai Guo, Sarah E. Elzinga, ..., Masha G. Savelieff, Junguk Hur, Eva L. Feldman

efeldman@umich.edu

Highlights

HFD induces obesity but does not alter microglia morphology by 1 month

HFD alters microglial endoplasmic reticulum (ER) and ribosome pathways after 1 month

HFD dysregulates microglia-to-microglia immune signaling, particularly after 3 months

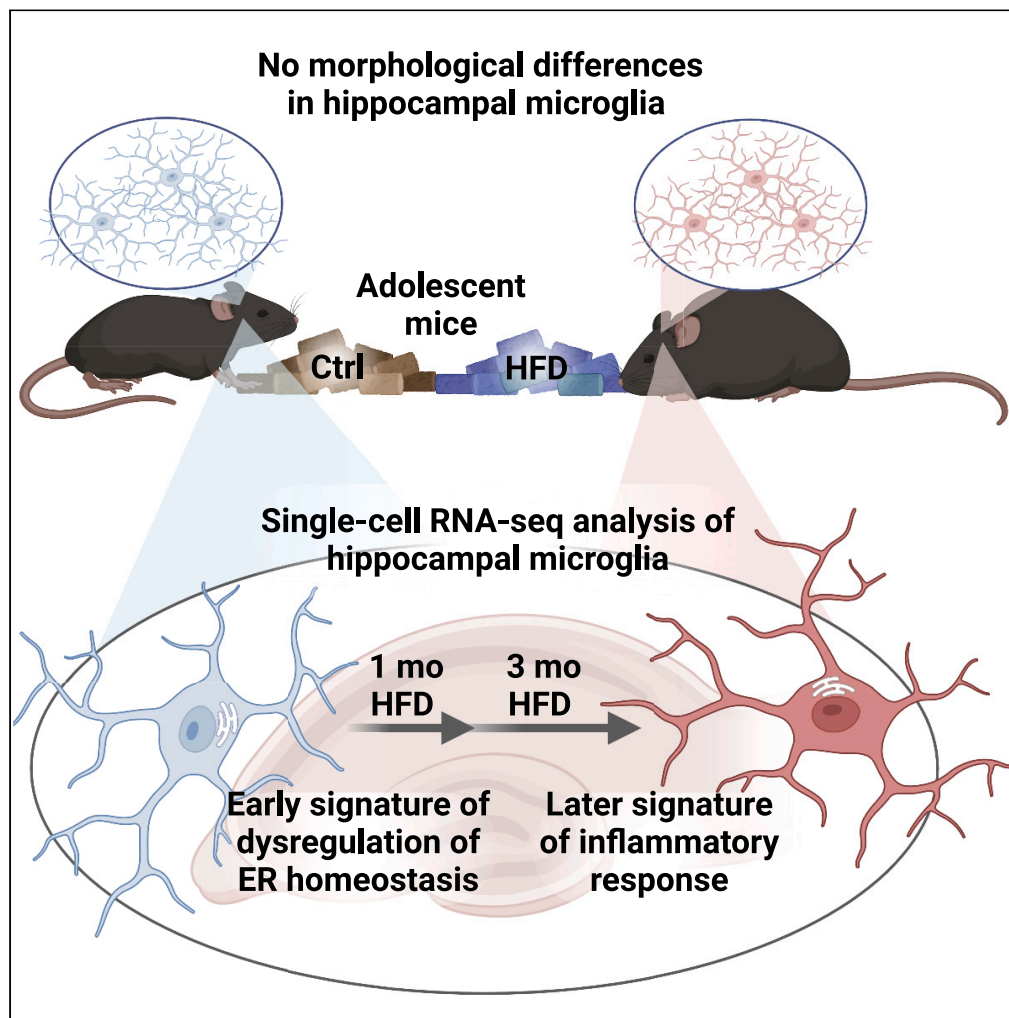HFD feeding induces an early ER response followed by a chronic inflammatory response

iScience

Article

Single-cell RNA sequencing identifies hippocampal microglial dysregulation in diet-induced obesity

Rosemary E. Henn,[1,2] Kai Guo,[1,2] Sarah E. Elzinga,[1,2] Mohamed H. Noureldein,[1,2] Faye E. Mendelson,[1,2] John M. Hayes,[1,2] Diana M. Rigan,[1,2] Masha G. Savelieff,[2] Junguk Hur,[3] and Eva L. Feldman[1,2,4,*]

SUMMARY

Obesity is a growing global concern in adults and youth with a parallel rise in associated complications, including cognitive impairment. Obesity induces brain inflammation and activates microglia, which contribute to cognitive impairment by aberrantly phagocytosing synaptic spines. Local and systemic signals, such as inflammatory cytokines and metabolites likely participate in obesity-induced microglial activation. However, the precise mechanisms mediating microglial activation during obesity remain incompletely understood. Herein, we leveraged our mouse model of high-fat diet (HFD)-induced obesity, which mirrors human obesity, and develops hippocampal-dependent cognitive impairment. We assessed hippocampal microglial activation by morphological and single-cell transcriptomic analysis to evaluate this heterogeneous, functionally diverse, and dynamic class of cells over time after 1 and 3 months of HFD. HFD altered cell-to-cell communication, particularly immune modulation and cellular adhesion signaling, and induced a differential gene expression signature of protein processing in the endoplasmic reticulum in a time-dependent manner.

INTRODUCTION

The global prevalence of obesity continues to rise. The World Health Organization estimates that global obesity rates tripled from 1975 to 2016, including an increase from 4% to 16% of overweight or obese children and teens.[1] This steep rise is concerning as the complications of obesity place an immense strain on patients and healthcare systems. Obesity is associated with cognitive impairment and structural brain changes in adults[2,3] and children and adolescents.[4–6] Midlife obesity also raises the risk of future dementia.[7,8] Currently, dementia management is limited to pharmacological and lifestyle interventions, which address only symptoms, not disease pathology. There is a critical need to understand the mechanisms underlying obesity-associated cognitive impairment across the lifespan.

Obesity activates microglia, the resident macrophage-like central nervous system (CNS) immune cells, which constitute a potential target for intervention. Most research has focused on hypothalamic microglial inflammation leading to the loss of regulatory mechanisms controlling satiety.[9–12] However, studies of obese mice demonstrate that microglia are also activated in the hippocampus, a limbic brain structure involved in memory and learning. Murine models of diet-induced obesity exhibit hippocampal inflammation after both acute[13,14] and chronic periods of high-fat diet (HFD).[15–17] Obese mice suffer from hippocampal-dependent cognitive deficits,[15,16,18] with hippocampal microglial morphology changes characteristic of pro-inflammatory activation after chronic HFD,[15,16] implicating microglia in cognitive impairment secondary to obesity.

In addition to potential morphological changes, obesity increases hippocampal levels of pro-inflammatory cytokines,[19] *e.g.* interleukin 1 beta (IL-1β) and tumor necrosis factor alpha (TNFα).[20] Inflammatory cytokines may activate microglia,[21] with a variety of other local or systemic signals such as dysregulated metabolites,[22] *e.g.* saturated fatty acids from HFD. Moreover, obesity increases peripheral immune cell recruitment,[23] and impairs blood-brain barrier function, facilitating entry of systemic inflammatory mediators.[24]

The mechanism of hypothalamic microglial activation and polarization during obesity has been well defined.[10,11,25] However, the hypothalamus is in direct contact with the circulation, and thus hypothalamic

[1]Department of Neurology, University of Michigan, Ann Arbor, MI, USA

[2]NeuroNetwork for Emerging Therapies, University of Michigan, Ann Arbor, MI, USA
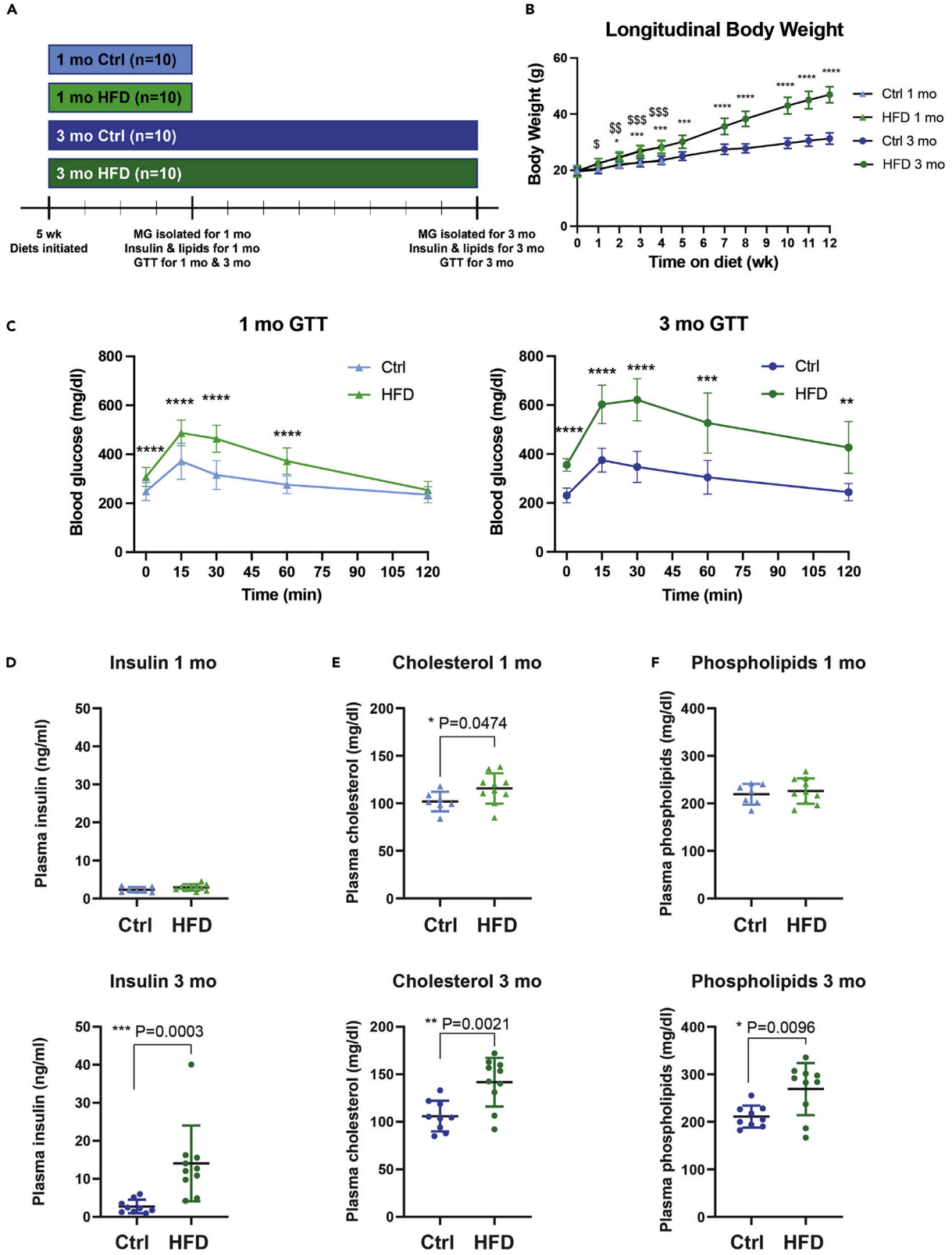
[3]Department of Biomedical Sciences, University of North Dakota, Grand Forks, ND, USA

[4]Lead contact

*Correspondence: efeldman@umich.edu

Figure 1. HFD induces obesity and dyslipidemia in mice

(A) Study design. Wild-type C57BL/6J mice aged 5 weeks were randomized to a high-fat diet (HFD) or control standard diet (ctrl). After 1 month (mo) or 3 (mo) of diet, HFD and control mice were sacrificed for microglial isolation and metabolic phenotyping (n = 10 per diet per time point).

(B) Longitudinal body mass; from 0 to 4 weeks (*i.e.*, 1 month time point) n = 20 per diet per time point (HFD, green; ctrl, blue); from 5 weeks onward, n = 10 per diet (HFD, green; ctrl, blue). $^\$p <0.05$, $^{\$\$}p <0.01$, $^{\$\$\$}p <0.001$, for HFD versus ctrl 1 month cohort; $^*p <0.05$, $^{***}p <0.001$, $^{****}p <0.0001$ for HFD versus ctrl 3 months cohort; repeated measures two-way ANOVA with Sidak's multiple comparisons test; data represented as mean $\pm$ SD.

(C) Glucose tolerance test (GTT); left panel for HFD (n = 20; light green) versus control (n = 20; light blue) at 1 month (triangles); right panel for HFD (n = 10; dark green) versus control (n = 10; dark blue) at 3 months (circles). Measures above the glucometer's upper threshold were set to the threshold, 750 mg/dL. Plasma (D) insulin, (E) cholesterol, and (F) phospholipids; top panels for HFD (n = 10; light green) versus control (n = 7; light blue) at 1 month (triangles); bottom panels for HFD (n = 10; dark green) versus control (n = 9; dark blue) at 3 months (circles). C to F, $^*p <0.05$, $^{**}p <0.01$, $^{***}p <0.001$, $^{****}p <0.0001$ for HFD versus control, by repeated measures two-way ANOVA and Sidak's multiple comparisons test for GTTs, by Welch's t-test for insulin, cholesterol, and phospholipids, and by Mann-Whitney test for insulin 3 months because data were not normally distributed; data represented as mean $\pm$ SD.

microglia are more directly exposed to saturated fatty acids. In contrast, hippocampal microglia are more protected from circulation, and therefore, their response to dietary saturated fatty acids and obesity over time may be less pronounced or exhibit a different time response versus hypothalamic microglia. In addition, most studies to date have examined single time points. Thus, there is a need to clarify the evolution of hippocampal microglial activation over time to determine the appropriate temporal window for intervention. There is also a need to address microglial heterogeneity, as a class of functionally diverse cells. Existing studies in the obesity field, such as those examining endoplasmic reticulum (ER) stress,[26] are limited by bulk hippocampal tissue analysis, which likely masks microglial-specific findings.
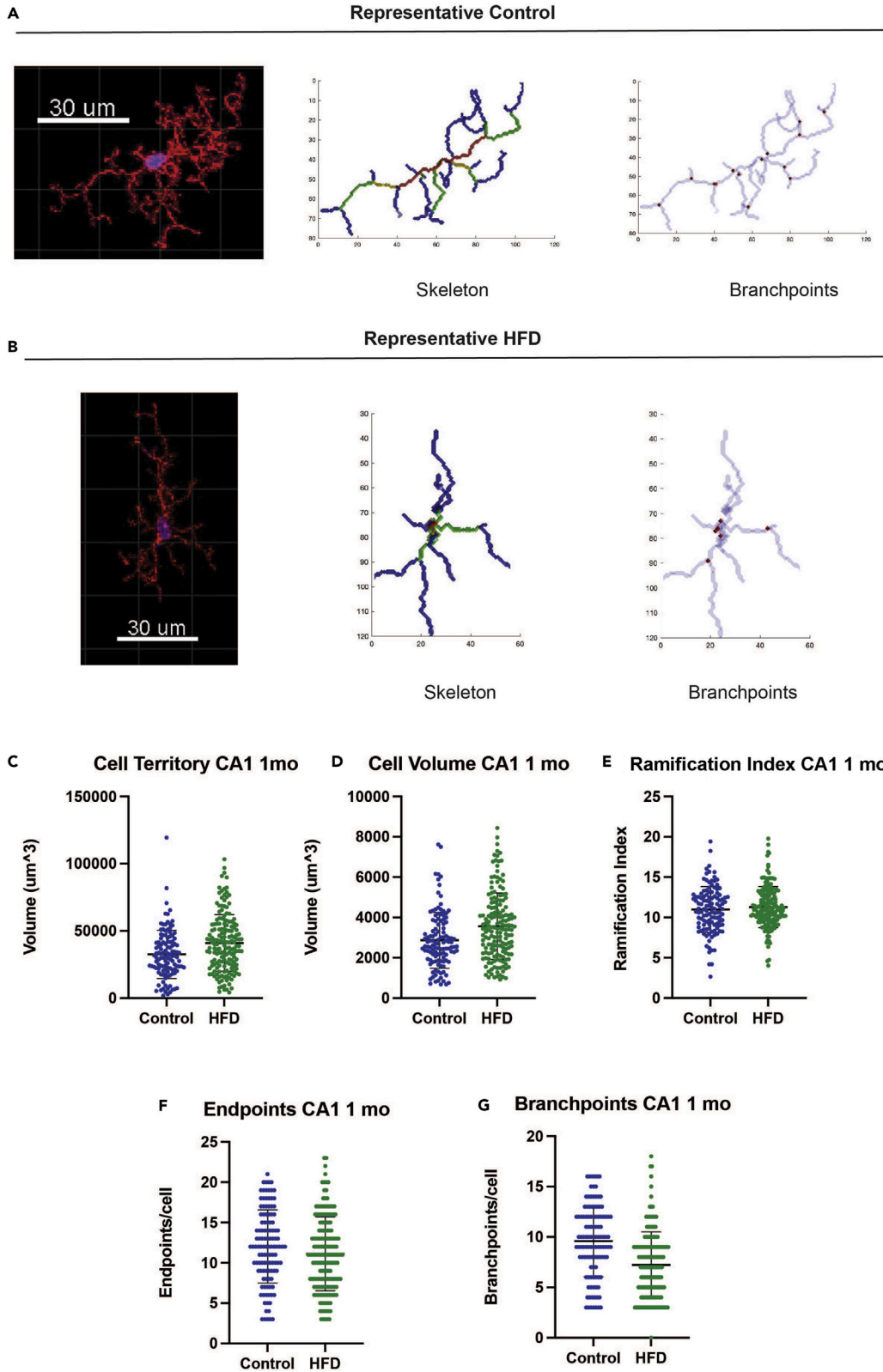
To address microglial heterogeneity, evolution of responses over time, and shortcomings from bulk analysis, we harnessed the power of single-cell RNA sequencing (scRNA-seq). We characterized, for the first time, the hippocampal microglial transcriptomic landscape at fine-grained single-cell resolution in the context of diet-induced obesity after 1 and 3 months (mo) of HFD. scRNA-seq identified obesity-associated dysregulated inflammatory pathways in microglia after 1 month or 3 months of HFD in wild-type C57B/L6J mice as they transitioned from adolescence to adulthood. In addition, we leveraged our single-cell dataset to investigate the dynamic immune cell-to-cell interplay, which is crucial for understanding subtle differences in microglial behavior in obesity. Our characterization of microglial activation states provides the foundation necessary to elucidate the role of microglia in hippocampal pathology in obesity.

RESULTS

HFD induces obesity but not early hippocampal microglial morphological activation

To determine the effect of obesity on hippocampal microglial activation, we utilized an established and deeply phenotyped mouse model of diet-induced obesity,[27,28] which we have previously used in our studies.[29] We fed 5-week-old male C57BL/6J mice (n = 10 per group) either a 60% HFD enriched with saturated fatty acids or a control diet containing 10% fat (Figure 1A). To determine time-dependent changes in microglia in response to HFD, mice were divided into two cohorts and fed for 1 month or 3 months. At the study endpoints, we isolated hippocampal microglia and performed scRNA-seq. HFD fed mice were heavier than control fed mice as early as after 2 weeks of diet (Figure 1B). After 1 month and 3 months, HFD mice had deficits in glucose homeostasis versus control mice, characterized by elevated peak blood glucose levels on glucose challenge, alongside a delayed return to baseline (Figure 1C). Baseline, *i.e.*, at 5 weeks of age, GTTs were indistinguishable between HFD and control groups (Figure S1A). Although glucose homeostasis was disrupted after 1 month of HFD, fasting plasma insulin did not increase in HFD mice relative to controls until 3 months (Figure 1D; p = 0.0003), recapitulating hyperinsulinemia in humans with chronic obesity.

We also examined basic plasma lipid profiles for cholesterol, triglycerides, phospholipids, and non-esterified fatty acids (NEFAs). Total plasma cholesterol was elevated in HFD mice after 1 month and 3 months diet (Figure 1E; p = 0.0474, p = 0.0021, respectively) and phospholipids after 3 months (Figure 1F; p = 0.0096). Diet did not affect triglyceride (Figure S1B) or NEFA (Figure S1C) levels. Collectively, these metabolic data demonstrate that HFD mice are obese and develop systemic metabolic dysfunction after just 1 month (*e.g.*, glucose intolerance, elevated cholesterol), which becomes more severe after 3 months (i.e., hyperinsulinemia, elevated phospholipids).

We previously reported hippocampal dependent cognitive deficits in short-term memory in a mouse model after 2 weeks, 6 weeks, and 24 weeks of HFD using a novel object recognition task.[18] Obesity is

A Representative Control

Skeleton Branchpoints

B Representative HFD

Skeleton Branchpoints

C Cell Territory CA1 1mo

D Cell Volume CA1 1 mo

E Ramification Index CA1 1 mo

F Endpoints CA1 1 mo

G Branchpoints CA1 1 mo

Figure 2. Obesity does not alter hippocampal microglial morphology at 1 month

(A) Representative 3D Morph[30] analysis for a control microglia from the hippocampal CA1 region, confocal microscopy (left), skeletonization (center), and branchpoints (right). Scale bar is 30 μm

(B) Representative 3D Morph analysis for an HFD microglia from the hippocampal CA1 region. Sections were stained for microglial Iba1 (594 nm, red channel) and with Hoechst nuclear staining (blue channel). Scale bar is 30 μm.

(C–G) Microglial (C) territorial volume, (D) cell volume, (E) ramification index (F) endpoints per cell, and (G) branchpoints per cell, all at 1 mo; left panels for control (ctrl; n = 3 animals, 3 images/animal; blue) versus HFD (n = 4 animals, 3 images/animal; green), each circle represents an individual cell. There were no significant differences in HFD versus control by linear mixed effects models with random animal-specific intercepts with t-test; data represented as mean ± SD.

associated with activated hippocampal microglia, assessed by morphological activation,[15,16] after 3 months of chronic HFD feeding. To address if hippocampal microglial changes occur earlier, like cognitive deficits, we quantified 3-dimensional (3D) microglial morphology after 1 month. Homeostatic microglia display complex branching patterns to surveil their environment, but environmental challenges trigger morphology shifts, characterized by smaller territorial volume and simpler branching patterns.

We performed 3D analyses on tissue sections stained by immunohistochemistry for the microglial marker ionized calcium binding adaptor molecule 1 (Iba1) using a modified 3D-Morph protocol.[30] 3D z-stack images of hippocampal tissue sections were acquired by confocal microscopy. After pre-processing in Imaris, images were run through 3D-Morph in MATLAB to measure territorial volume, cell volume, and branching parameters based on convex hull analyses and skeletonization[30] (representative cells, Figures 2A and 2B). After a 1-month diet, microglia in the CA1 region of the hippocampus from HFD-fed mice were not morphologically distinct from control microglia. Territorial volume (p = 0.16), the 3D space taken up by the cell body and all its branches, cell volume (p = 0.26), defined as the volume of the soma and branches themselves, and ramification index (p = 0.52), defined as the territorial volume divided by the cell volume, did not differ by diet (Figures 2C–2E). There was also no difference in the number of endpoints (p = 0.42) and branchpoints (p = 0.08) (Figures 2F and 2G); however, there was a trend toward fewer branchpoints per cell in HFD microglia.

Microglial heterogeneity remains constant in HFD and control mice

Next, we investigated the microglial single-cell transcriptome to understand how hippocampal microglia are activated to contribute to obesity associated cognitive impairment. To characterize transcriptomic heterogeneity of the microglial landscape, we performed scRNA-seq on microglia isolated from the hippocampi of HFD and control mice (n = 6 per group) after 1 month and 3 months (Figure 3A). We performed a papain enzymatic digestion followed by serial trituration to prepare a single cell suspension from the hippocampus. We enriched for microglia by applying a 40% Percoll centrifugation to our cells and collecting the cell pellet, and further purified by fluorescence-activated cell sorting (FACS). We sorted CD11b⁺/CD45^low double-positive cells, representing microglia, rather than CD11b⁺/CD45^high cell surface markers, which represent macrophages. Sorted cells were sequenced on the 10X Chromium platform and RNA reads were quality filtered before mapping to the mouse reference genome. We used CellRanger Count to prepare sample files, which were read into Seurat. Cells were excluded from downstream analysis based on criteria outlined in the STAR Methods section. In total, 4,555 HFD and 4,945 control cells were included in the analysis at 1 month, and 1,292 HFD and 1,255 control cells at 3 months. Data were normalized to reduce the effects of differing cell numbers on expression levels in downstream analyses and ratios were reported for changes in cell type rather than changes in absolute number. To determine the success of FACS, we examined expression of the CD11b gene, *Itgam*, and the CD45 gene, *Ptprc*, which were expressed by most cells, suggesting a successful cell sort (Figure S2A).

Next, we performed principal component analysis to reduce data dimensionality and then analyzed and visualized clusters using Uniform Manifold Approximation and Projection (UMAP). We identified eleven cell clusters (Figures 3B andS3 for UMAP plots per mouse), which were characterized by cell-specific markers found using the FindAllMarkers function in Seurat (Figure 3C). We reviewed previously published datasets and leveraged the CellMarker and PanglaoDB databases to assign cell type identities to each cluster. As anticipated, most clusters, seven out of eleven, were microglial subtypes, of which three were homeostatic microglia (HMG), HMG1, 2, 3. The remaining microglial subtypes were inflammatory microglia (InflamMG, expressing C-C motif chemokine ligand 4 [Ccl4] and Ccl3, Figure 3D), interferon-related microglia (IfnMG, expressing interferon induced protein with tetratricopeptide repeats 2 [Ifit2] and Ifit3, Figure 3D), proliferating microglia (ProlifMG, expressing DNA topoisomerase II alpha [Top2a], Figure 3D,
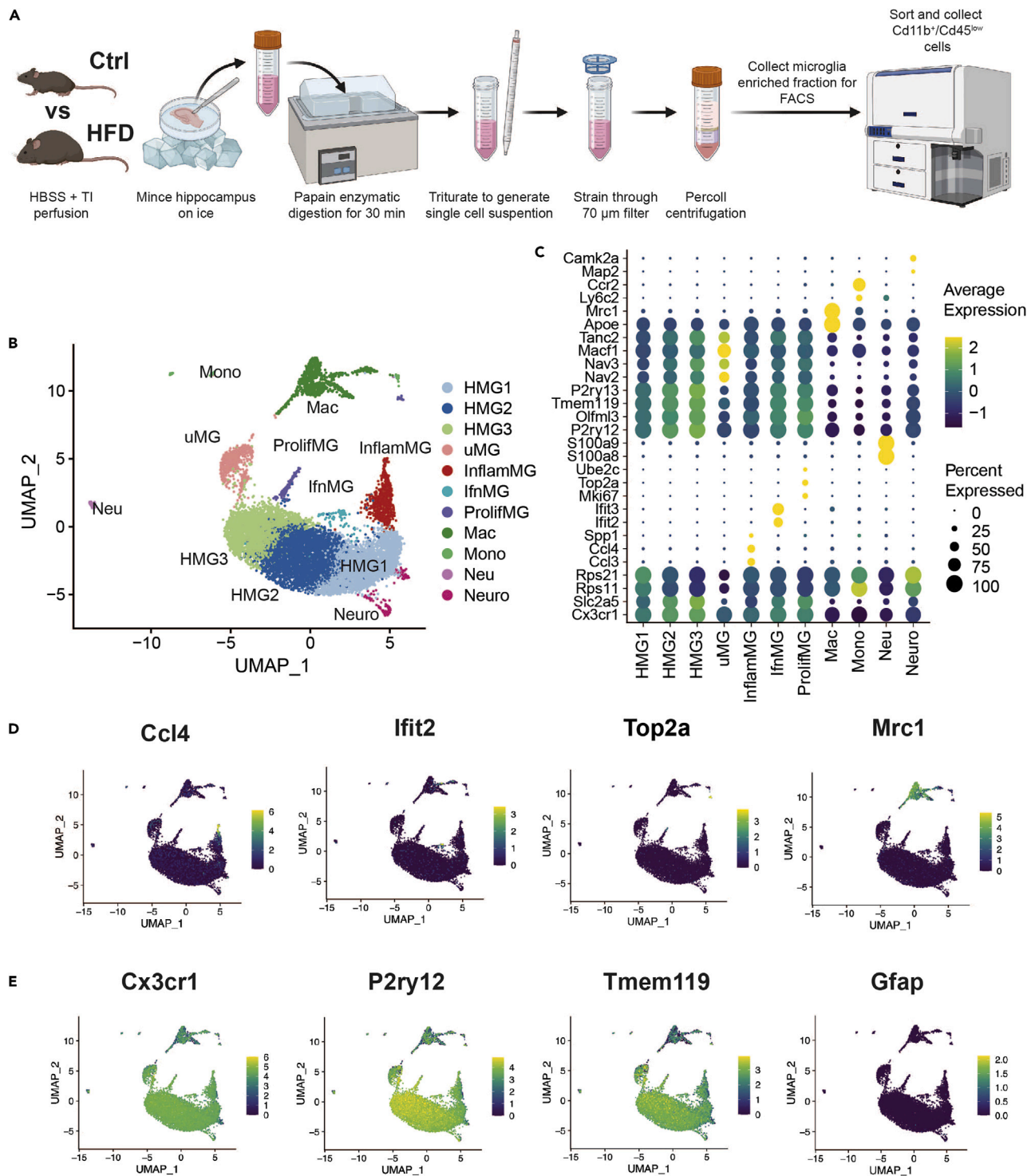
Figure 3. Isolated cells cluster into eleven distinct populations

(A) Diagram of microglial isolation protocol; cells were isolated from 6 mice per group. Created with BioRender.com.

(B) Uniform Manifold Approximation and Projection (UMAP) shows 11 clusters, which represent homeostatic microglia 1 (HMG1), HMG2, HMG3, macrophages (Mac), uMG (unknown, functionally undescribed), inflammatory microglia (InflamMG), proliferating microglia (ProlifMG), neurons (Neuro), interferon-related microglia (IfnMG), neutrophils (Neu), and monocytes (Mono). UMAP plot represents 4,555 HFD and 4,945 control cells at 1 month, and 1,292 HFD and 1,255 control cells at 3 months.

Figure 3. *Continued*

(C) Dot plot of markers used to assign cluster identity. Dot size represents the percentage of cells from a given cluster expressing the marker, dot color represents average expression relative to all other clusters.

(D) UMAP plots by markers that differentiated various clusters, InflamMG by chemokine *Ccl4* (C-C motif chemokine ligand 4), IfnMG by interferon-induced *Ifit2* (interferon induced protein with tetratricopeptide repeats 2), ProlifMG by DNA topoisomerase *Top2a* (DNA topoisomerase II alpha), and macrophages by immunomodulating *Mrc1* (mannose receptor C-type 1).

(E) UMAP plots with expression of microglial (*Cx3cr1*, CX3C chemokine receptor 1; *P2ry12*, purinergic receptor P2Y12; *Tmem119*, transmembrane protein 119) versus astrocytic (*Gfap*, glial fibrillary acidic protein) markers shows a relatively pure microglia isolation. UMAP plot for another microglial marker, *Aif1* (allograft inflammatory factor 1), the gene encoding Iba1 protein, is shown in Figure S2.

and marker of proliferation Ki-67 [Mki67]), and a functionally undescribed subtype labeled "uMG" for 'un-described microglia' (Table S1).

In addition to the microglia subtypes, we also identified macrophages (Mac, expressing mannose receptor C-type 1 [Mrc1], Figure 3D), monocytes (Mono, expressing C-C motif chemokine receptor 2 [Ccr2] and lymphocyte antigen 6 complex, locus C2 [Ly6c2], UMAP in Figure S4, features in Figure 3C), neutrophils (Neu, expressing S100 calcium binding protein A8 [S100a8] and S100a9, UMAP in Figure S4, features in Figure 3C), and neurons (Neuro, expressing calcium/calmodulin dependent protein kinase II alpha [Camk2a] and microtubule-associated protein 2 [Map2], UMAP in Figure S4, features in Figure 3C). Most sequenced cells expressed microglial markers *Cx3cr1*, *P2ry12* (Figures 3E and S5 for *Cx3cr1* UMAP plots per mouse), and *Aif1* (gene coding for Iba1; Figure S2B) and the microglial-specific gene *Tmem119* (Figure 3E), as expected, because we enriched for microglia. Furthermore, the analyzed cells showed almost no expression of the astrocyte specific gene *Gfap* (Figure 3E) or oligodendrocyte specific gene *Olig2* (Figure S2C), indicating the absence of astrocytes and oligodendrocytes among isolated cells, as anticipated following a microglial sort. Cells expressed very low levels of the neuronal specific gene *Rbfox3* (Figure S2C), suggestive of a very small neuronal population.

All seven microglial and four additional cell type clusters were present in both HFD and control groups (Figure 4A), and at both 1 month and 3 months. Although all cell clusters were represented in all experimental groups, we assessed the proportion of each cell cluster by diet or age. Cluster proportions were similar between HFD and control groups at 1 month and 3 months (Figure 4B). In all experimental groups, the largest proportion of cells comprised homeostatic microglia, HMG1, 2, and 3 at both 1 month (HFD 77.8% versus control 76.9%) and 3 months (HFD 69.4% versus control 65.3%). Macrophages were the second most abundant cell type after HMGs at 1 month (HFD 7.1% versus control 7.5%) and 3 months (HFD 12.2% versus control 12.4%). Other microglial subtypes (uMG, InflamMG, ProlifMG, and IfnMG) ranged from 0.8% to 8.6% of all cells in HFD and control conditions at 1 month and 3 months.

Obesity dysregulates microglial inflammatory cell-to-cell signaling

Microglia are immune cells that constantly survey the CNS environment and respond to external signals.[31–33] Thus, we examined the effect of diet-induced obesity on cell-to-cell communication within our single-cell dataset. To do so, we utilized CellChat,[34] a tool that leverages a database of over 2,000 ligand and receptor pairs and scRNA-seq data to infer intercellular communication. We first looked at information flow of intercellular signaling pathways in HFD and control conditions at 1 month and 3 months (Figures 5A and 5D), which is based on a summation of probabilities of pathway communication for all cell type pairs. For each pathway, CellChat also identifies the ligand-receptor gene pairs contributing to pathway signaling, which is visualized in circle plots of cell types that send and receive signals for the given pathway (Figures 5B, 5C, 5E, 5F, and S6 for ligand-receptor expression).

Information flow at the 1 month time point was higher in 23 pathways in HFD versus control cells and 12 pathways in control versus HFD cells (Figure 5A). In some instances, signaling pathways were only detected in cells of one diet group, *e.g.*, type-1 interferon (IFN-I) signaling at 1 month in HFD cells. The pathways with microglia-to-microglia signaling that were elevated in HFD at 1 month fell into a few broad categories. 'CDH', 'ICAM1,' 'PECAM1', 'HSPG, and 'CD200' ligands are cell surface glycoproteins with various immune regulatory roles, including T cell co-stimulation,[35] cellular adhesion,[36] microglial pro-inflammatory activation,[37–39] as well as inhibition of microglial activation in the case of CD200.[40] The 'IFN-I' ligand is a cytokine involved in canonical pro-inflammatory signaling. 'EGF', 'GRN', and 'TGFb' ligands are growth factors, and loss of microglial progranulin and granulin signaling has been extensively studied in frontotemporal
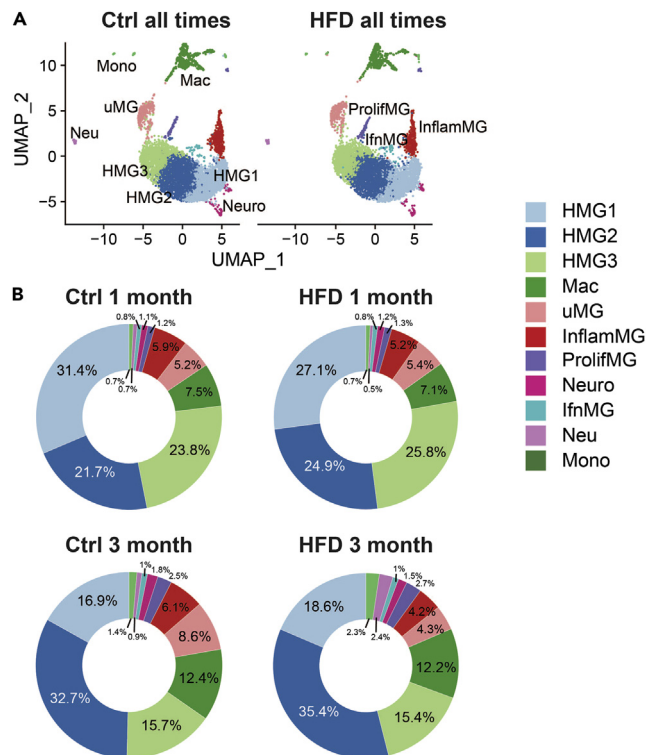
Figure 4. Microglial heterogeneity remains constant in HFD versus control mice

(A) UMAP of HFD (5,847 total cells) versus control (ctrl; 6,200 total) at both time points isolated from n = 6 mice per group.
(B) Top panel: Circle chart of all 11 cell types by percentage at 1 month for HFD (left; 4,555 total cells) versus control (right; 4,945 total cells). Bottom panel: Circle chart of all 12 cell types by percentage at 3 months for HFD (left; 1,292 total cells) versus control (right; 1,255 total cells).

dementia[41] and neurodegeneration.[42] Finally, the 'SEMA6' ligand is a transmembrane protein with a known role in axon guidance.[43]

'HSPG' and 'IFN-I' were the sole pathways driven by microglia-to-microglia signaling with information flow turned on in HFD cells at 1 month (Figures 5B and 5C). For 'HSPG' signaling, InflamMG signaled to HMG3, HMG2, and ProlifMG, with autocrine signaling to itself, and IfnMG cells signaled to InflamMG and ProlifMG (Figure 5B; top). Signaling was mediated between the ligand heparan sulfate proteoglycan 2 (Hspg2) and its receptor, dystroglycan 1 (Dag1) (Figure 5B; bottom). The interferon ('IFN-I') signaling pathway network in HFD cells at 1 month was more complex and involved connections among multiple cell types, including non-microglia cells. 'IFN-I' signaling originated from ProlifMG, Mac, Mono, IfnMG, InflamMG, HMG3, HMG2, and HMG1) (Figure 5C). Because we enriched for microglia using CD11b$^+$/CD45^{low} FACS, the non-microglial immune cells we isolated may comprise a biased sampling of the true populations. Owing to this potential bias and the likelihood that they do not represent the full diversity of monocytes, neutrophils, macrophages, and neurons, it is difficult to draw firm conclusions regarding signaling networks involving these cell types as the senders and/or receivers. However, we can determine that IFN-I signaling involves a dynamic interplay between multiple cell types, highlighting the value of cell-to-cell communication analysis in the context of microglial mediated pathology.

Information flow at the 3 months time point was higher in 27 pathways in HFD versus control cells and 10 pathways in control versus HFD cells (Figure 5D). Again, in some cases, signaling pathways were only detected in cells of one diet group, *e.g.*, 'IL6' signaling at 3 months in HFD cells. At 3 months, HFD turned on microglia-to-microglia signaling of 'IL6', 'PDGF' (Figures 5E and 5F), 'KIT', 'VISTA' (Figure S7A), 'HSPG', and 'LAMININ' pathways. The pathways elevated in HFD cells relative to controls containing microglia-to-microglia network signaling included 'CD86', 'ICOS', 'CD200', 'SEMA6', 'PROS', 'CD48', 'CADM' (Figures S7B and S7C), 'TGFb', and 'GRN'. Like at 1 month, signaling pathways ligands included growth
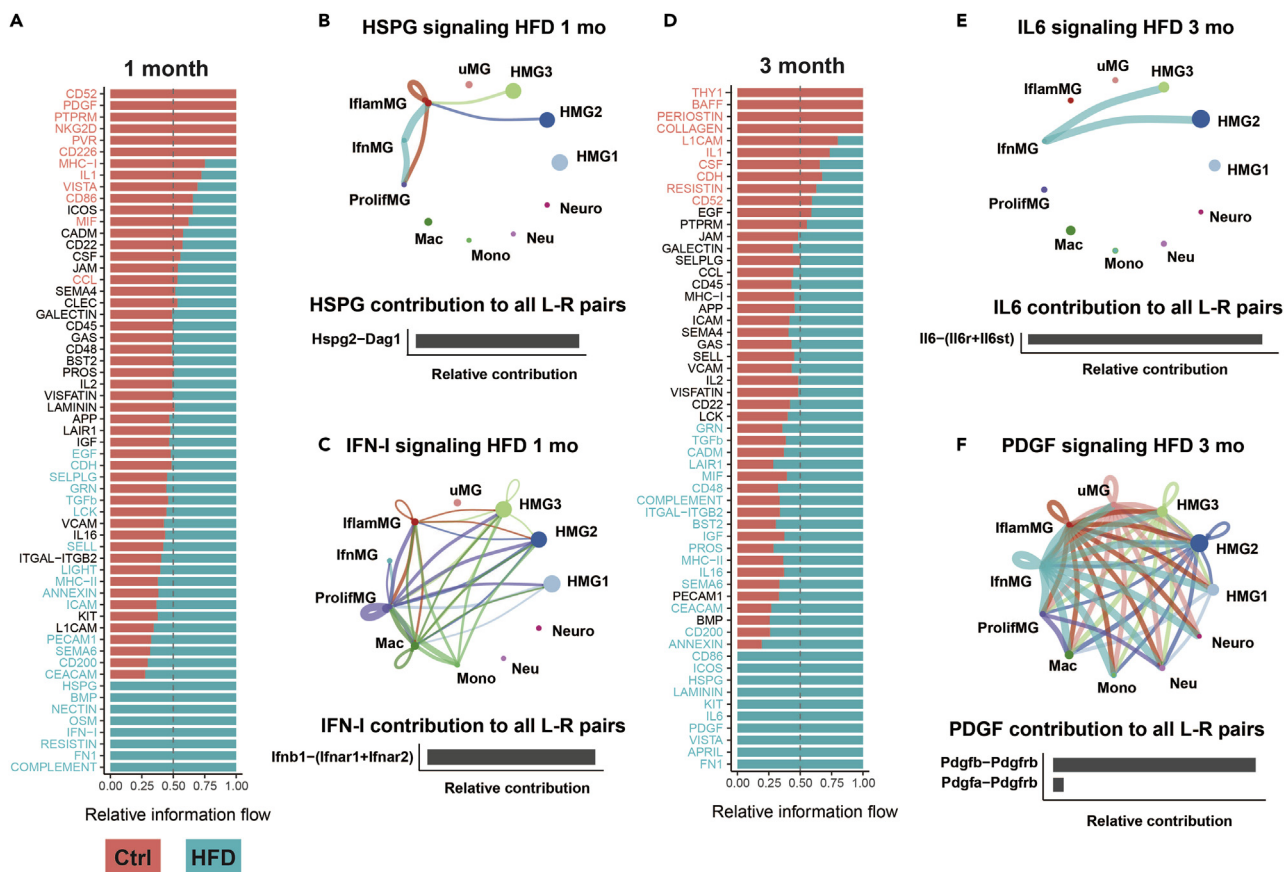
Figure 5. Cell-to-cell communication analyses reveal HFD specific intercellular communication pathways

(A) Information flow charts at 1 month for HFD (blue) versus control (ctrl; red) generated by CellChat. Teal bars represent information flow in HFD cells (4,555 total cells), red bars represent information flow in control cells (4,945 total cells). Signaling pathways in teal text have significantly higher information flow in HFD cells relative to control, signaling pathways in red text have significantly higher information flow in control cells, and signaling pathways in black text are not significantly different between groups; vertical dashed lines represent information flow equal in both HFD and control.

(B and C) Circle plots of cellular signaling interactions (top) and their top contributing ligand-receptor (L-R) pairs (bottom) for pathway networks involving (B) HSPG for HFD at 1 month and (C) IFN-I for HFD at 1 month. Dots in circle plots represent cell populations with color codes matching UMAP clusters; strokes represent communication between distinct cell populations and loops represent signaling within cell populations. Stroke and loop colors reflect the cluster sending the signal, and thickness reflects strength of the signaling pair.

(D) Information flow chart at 3 months for HFD (blue; 1,292 total cells) versus control (ctrl; red; 1,255 total cells).

(E and F) Circle plots (top) and top contributing L-R pairs (bottom) for pathway networks involving (E) IL6 for HFD at 3 months and (F) PDGF for HFD at 3 months.

factors, e.g., 'PDGF', 'KIT', 'TGFb', and 'GRN', and glycoproteins with immunomodulatory functions, e.g., 'HSPG' and 'CD200'. 'IL6' and 'KIT' ligands are cytokines, and other ligands are cell surface immunomodulatory antigens, e.g., 'CD86', 'ICOS', 'CD48', and 'VISTA'. IL-6, a cytokine with context-dependent pro- or anti-inflammatory effects,[44] was expressed by IfnMG and its receptor by HMG2 and HMG3 (Figure 5E). We found HFD turned on PDGF signaling at 3 months (Figure 5F). Several microglia subtypes (InflamMG, HMG1, HMG2, HMG3, ProlifMG, IfnMG, uMG) expressed the platelet-derived growth factor (PDGF) ligand and signaled to other microglia, as well as to macrophages, neutrophils, monocytes, and neurons. PDGF is a mitogen with well-studied roles in development and wound healing, yet has detrimental effects in various disease contexts, such as cancer and atherosclerosis.[45,46]

Obesity dysregulates microglial ER homeostasis

The results from CellChat yielded insight into the effects of obesity on microglial cell-to-cell communication. However, we were also interested in the dysregulated intracellular processes to identify potential drivers of an activated state. To accomplish this goal, we performed differentially expressed gene (DEG) analysis for all microglia types combined in HFD versus control using DESeq2. There were 89 DEGs after
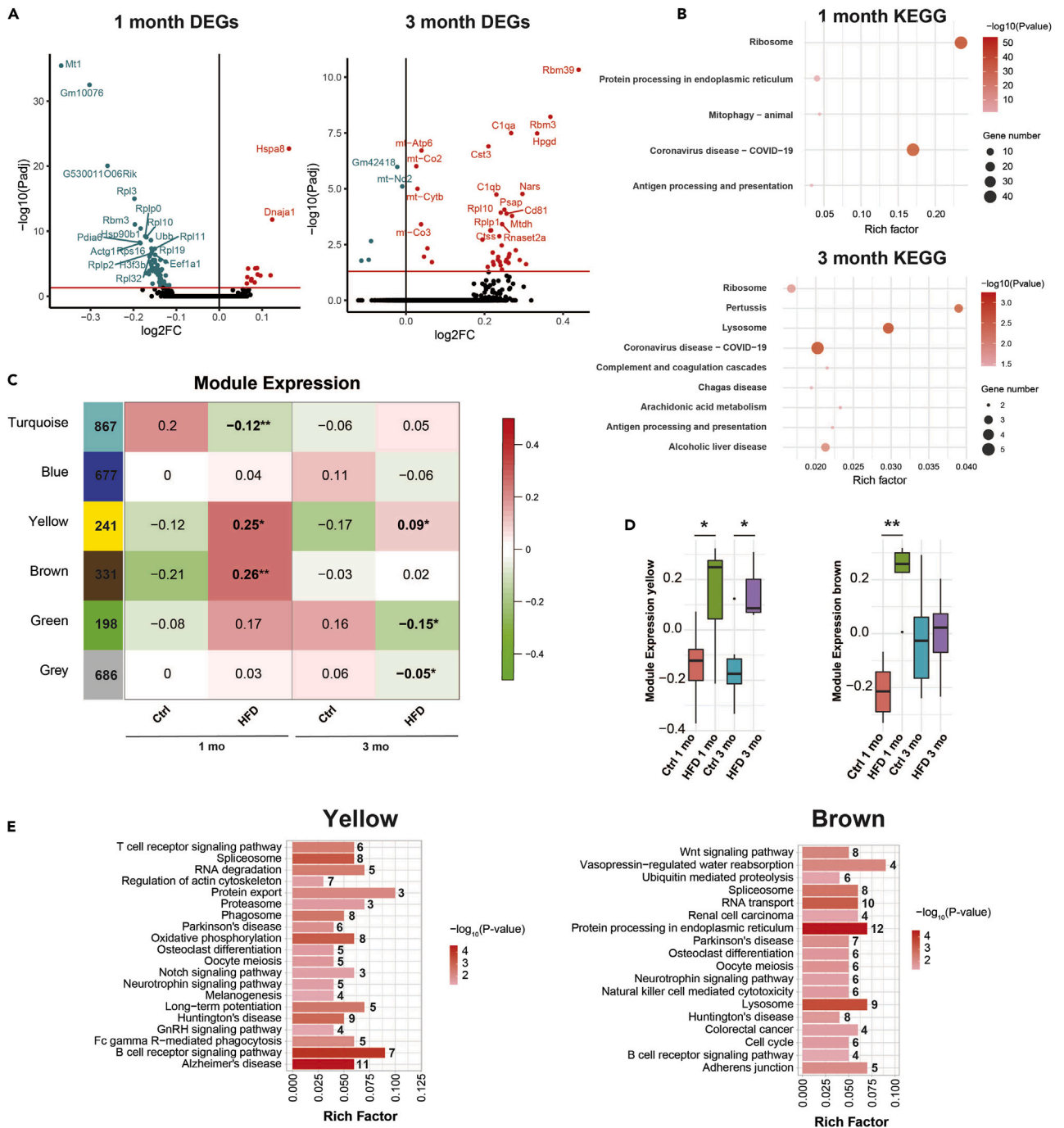
Figure 6. HFD dysregulates protein processing in the ER across microglial subtypes

(A) Volcano plots of differentially expressed genes (DEGs) in HFD versus control (ctrl) at 1 month (left) and 3 months (right) for all microglia subtypes combined with top 20 annotated DEGs. Analysis included 4,450 ctrl 1 month, 1,048 ctrl 3 months, 4,121 HFD 1 month, and 1,054 HFD 3 months microglia. Significant DEGs above the horizontal red line based on P-adjusted <0.05, blue dots represent significantly downregulated in HFD, red dots represent significantly upregulated in HFD. FC, fold-change.

(B) KEGG pathway analysis of DEGs in HFD versus control at 1 month (top) and 3 months (bottom). Dot color represents-$\log_{10}$(P-value) from least significant (light pink) to most significant (red); dot size represents gene number, the number of significant DEGs in the KEGG pathway; rich factor represents the fraction of significant DEGs among all genes in the KEGG pathway.

(C) WGCNA modules by color, turquoise, yellow, brown, green, blue, with number of genes assigned to each module (column 1), and corresponding heatmap of median module expression by condition. The gray module comprises genes that did not cluster into a co-expression module. Significant differences in expression of genes in modules between experimental groups by Kruskal-Wallis, *p <0.05, **p <0.01.

Figure 6. Continued

(D) Boxplots of yellow and brown module expression. Significant differences by Kruskal-Wallis, *p <0.05, **p <0.01. Boxplot height represents the interquartile range, horizonal line the median, and whiskers the minimum and maximum values of expression.

(E) KEGG pathway analysis of genes in HFD versus control from the yellow (left) and brown (right) modules. Bar color represents-log$_{10}$(P-value) from least significant (light pink) to most significant (red); bar length represents the number of genes in the KEGG pathway, annotated with a number; rich factor represents the fraction of genes among all genes in the KEGG pathway.

1 month HFD, and 46 DEGs after 3 months (adjusted P-value <0.05) (Figure 6A, Table S2). To identify the biological significance of these DEGs, we performed Encyclopedia of Genes and Genomes (KEGG) enrichment analysis (Figure 6B). Five pathways were identified at 1 month; 'ribosome' and 'COVID-19' contained the same genes, which were all ribosomal and included *Rpl3*, *Rplp0*, *Rpl10*, *Rps16*, *Rpl11*, among others. 'Protein processing in the ER contained *Hspa8*, *Dnaja1*, *Hsp90b1*, *Pdia6*, *Calr*, *Hspa5*, and *Dnajb1*. 'Mitophagy-animal' and 'antigen processing and presentation' contained only three genes each. Performing KEGG analysis for 3 months was less informative, because of few DEGs, only 46, KEGG enrichment analysis at 3 months yielded 'lysosome,' 'COVID-19,' 'pertussis,' 'alcoholic liver disease,' 'ribosome,' 'arachidonic acid metabolism,' 'antigen processing and presentation,' 'complement and coagulation cascades,' and 'Chagas disease.' However, there were no more than five genes in each KEGG pathway, including *C1qa* and *C1qb* complement genes, which were present in five of the nine pathways.

Next, we identified DEGs in HFD versus control for each of the 11 cell types at both 1 month and 3 months. Overall, few DEGs (adjusted P-value <0.05) were identified, with 0 DEGs for most comparisons (Table S3). DEGs for HFD versus control were identified for HMG1 (18 DEGs), HMG2 (8 DEGs), HMG3 (8 DEGs), and Mac (3 DEGs) at 1 month. At 3 months, DEGs were identified for HMG1 (1 DEGs), HMG2 (8 DEGs), and HMG3 (1 DEG). For both the cluster specific and all microglia combined analyses, there were more DEGs at 1 month than 3 months. The cluster specific analysis detected DEGs in HFD versus control only in HMG populations and macrophages. Although there were too few genes to perform KEGG on cluster specific DEGs, we found again, that protein processing in the ER genes were represented. At 1 month, ER related DEGs included *Hspa8*, *Hsp90b1*, and *Dnaja1* for HMG1, *Hspa8* and *Calr* for HMG2, and *Hspa8*, *Dnaja1*, and *Pdia6* for HMG3. The DEGs in the macrophage group were *H3f3b*, *Ucp2*, and *Gm10076*. At 3 months, *Hsp90ab1* and *Hsp90aa1* were DEGs in HMG2.

Owing to the similarity among UMAP clustered HMG subtypes, and because most cluster specific DEGs were identified in HMGs, we next considered the three homeostatic microglia subtypes as a single cluster and performed DESeq2 analysis. We identified 96 DEGs at 1 month and 12 DEGs at 3 months in all three homeostatic microglia subtypes combined (Table S4). KEGG analysis at 1 month in this subset of HMGs again showed enrichment in 'ribosome,' 'COVID-19,' and 'protein processing in the ER' as well as in 'prostate cancer' and 'salmonella infection.' Homeostatic microglia make up the largest proportion of all microglia, so it is expected that HMG DEGs reflect the DEGs for the combined microglia analysis.

Because few DEGs were identified between HFD and control groups, we implemented an additional approach to examine differences between groups and infer potential biological significance. We performed weighted gene co-expression network analysis (WGCNA), an unsupervised correlation analysis, to identify co-expressed gene modules across all samples, including genes for all cell types. WGCNA identifies co-expression networks, aka modules, which differ significantly between HFD versus control, rather than individual DEGs by DESeq2 analysis. Analysis of 1 month and 3 months samples yielded five co-expression modules and 1 module of genes (gray module) that were not assigned to a co-expression module (Figure 6C; module dendrogram, Figure S8A). Four modules, turquoise, yellow, brown, and green, differed significantly between HFD and control groups. The turquoise module, containing 867 genes, had reduced expression in HFD at 1 month (p = 0.0087), the yellow module, containing 241 genes, had elevated expression in HFD at 1 month (p = 0.041) and 3 months (p = 0.026), the brown module, containing 331 genes, had elevated expression in HFD after 1 month (p = 0.0022), and the green module, containing 198 genes, had reduced expression in HFD at 3 months (p = 0.041) (Figures 6D and S8B). We next performed KEGG enrichment analysis on each module. The yellow module was enriched for genes in a variety of biological pathways, including 'Alzheimer's disease', containing the genes *Psenen*, *Ndufb5*, *Atp5o*, *Gnaq*, *Ndufs8*, *Ndufa5*, *Mapk3*, *Ndufs4*, *Atp5g3*, *Ppp3r1*, and *Psen1* (Table S5), and 'B cell receptor signaling pathway' (Figure 6E). The brown module was enriched for 'protein processing in the ER' which contained 12 genes related to the ER stress response, *Hspa8*, *Nfe2l2*, *Selenos*, *P4hb*, *Dnaja1*, *Ssr1*,
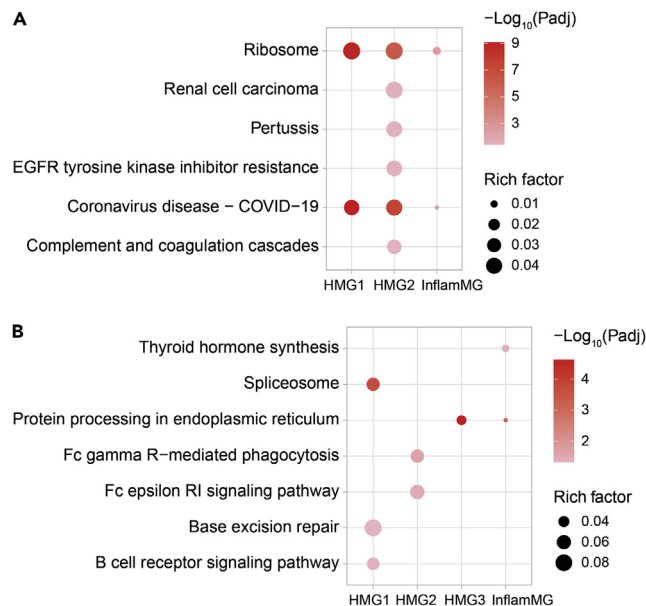
Figure 7. Obesity correlates with distinct transcriptomic signatures in various microglia types
KEGG pathway enrichment analysis of transcripts (with Benjamini-Hochberg corrected P-value<0.05) that correlate
(A) positively and (B) negatively with body weight in various microglia types [homeostatic microglia 1 (HMG1), HMG2,
HMG3, inflammatory microglia (InflamMG), uMG (unknown, functionally undescribed)]. Dot color represents-$\log_{10}$(Padj)
from least significant (light pink) to most significant (red); rich factor represents the fraction of significant body weight
correlated transcripts among all genes in the KEGG pathway. Padj, adjusted P-value.

Edem1, Man1c1, Eif2s1, Ube2j1, Erlec1, and *Dnajb1* (Table S5). Some of these genes have been identified
as relevant to microglia in obesity by other studies in bulk or functional studies, such as heat shock protein
70 (*Hspa8*), HSP40 (*Dnaja1, Dnajb1*),[47] and Nrf2 (*Nfe2l2*).[48] The turquoise module was most significantly
enriched in 'ribosome' and 'oxidative phosphorylation' genes, and the green module in 'protein process-
ing in the ER' genes (Figures S8C and S8D).

Obesity correlates with distinct transcriptomic signatures in various microglia types

Finally, because our focus was the impact of obesity on microglia transcriptomic signatures, we examined
the correlation of obesity, as it progress from 1 month to 3 months, to transcriptomic profiles in distinct
microglia clusters. We performed a Spearman correlation analysis of body weights at 1 month and 3 months
to transcript levels at 1 month and 3 months in all cell clusters (Figure S9, Table S6). We found several genes
whose expression levels correlated positively with body weight in various cell clusters, e.g., *C1qc* in HMG1
and 2, or negatively, *e.g., Hsp90b1* in HMG1, 2, and 3, InflamMG, and Mac. To infer biological meaning, we
next performed separate KEGG pathway enrichment analysis of positively (Figure 7A) and negatively (Fig-
ure 7B) correlated transcripts (Table S7). The most significant pathways that correlated positively with
obesity were 'ribosome' and 'COVID-19' in HMG1 and 2 and InflamMG. The 'COVID-19' pathway contains
complement and ribosome genes. Importantly, rich factors were low, so only a few genes in these KEGG
pathways were activated with obesity. The most significant pathways that associated negatively with
obesity were 'protein processing in ER' in HMG3 and InflamMG, 'spliceosome' in HMG1, and 'Fc gamma
R—mediated phagocytosis' in HMG2. Notably, rich factors were low, indicating that only a few genes corre-
lated with body weight of all genes present in the KEGG pathway. The genes (Figure S9) and pathways (Fig-
ure 7) that correlated with body weight overlapped with the DEGs and pathways at 1 month and 3 months
(Figures 6A and 6B), suggesting that progressive obesity particularly influences these genes.

DISCUSSION

Rates of obesity are climbing,[1] alongside rises in associated complications, such as cognitive impair-
ment.[2,8] Thus, there is a need to understand the pathophysiology of cognitive deficits secondary to obesity
to intervene. Through their contribution to cognitive impairment in obesity,[15] microglia serve as a potential

therapeutic target, although the mechanisms of microglial activation in this context remain incompletely understood. In this study, we used scRNA-seq to determine the effect of obesity over time on the hippocampal microglial transcriptome. scRNA-seq allowed us to probe the heterogeneity of microglial populations and identify unique cellular processes and inflammatory pathways that are dysregulated in obesity. We, for the first time in the adolescent and adult C57BL/6J hippocampus, identified seven microglial subtypes, with three other immune cell types and neurons. All cell types were present in HFD and control groups at 1 month and 3 months diet, and diet did not affect cell type proportion. Conversely, cell-to-cell communication analysis revealed a functionally diverse set of signaling pathways, which differed significantly between diet groups. In particular, HFD dysregulated microglial signaling involved in immune modulation. DEG analysis with KEGG pathway enrichment revealed a signature of dysregulated ER genes in HFD microglia, which was independently confirmed by a separate WGNCA analysis.

We studied the effect of obesity on microglial activation in a mouse model of diet-induced obesity,[29] which displays hippocampal-dependent cognitive impairment.[18] HFD mice were heavier than their control counterparts after only 2 weeks of diet and went on to develop progressive metabolic dysfunction, including hyperinsulinemia and dyslipidemia, as occurs in human obesity. Because we expected that the immune response would evolve over time, we assessed morphological activation early on at 1 month. We found that HFD did not alter microglial morphology in the hippocampal CA1 region at 1 month. This finding is not unexpected at 1 month, because previously published studies showed HFD-induced morphological activation of microglia, quantified in part by fewer primary cell processes, occurs later at 3 months in the hippocampal dentate gyrus and CA1.[15,16] Although there was no significant difference in branchpoints per cell between groups, there was a trend toward fewer branchpoints in HFD microglia. Further studies are required to determine whether this trend might represent the start of ramification reduction, which then continues over time.

Although we did not observe hippocampal microglial morphological activation, scRNA-seq enabled us to investigate early transcriptomic changes across diverse microglial subtypes. No studies, to our knowledge, had examined hippocampal microglial heterogeneity in obesity, and no microglial scRNA-seq studies have focused on the healthy hippocampus in the C57BL/6J mouse. Thus, we performed scRNA-seq on microglia isolated from the hippocampi of obese and lean mice after 1 month and 3 months. We sought to determine the effect of obesity on microglial activation and its temporal evolution at the transcriptomic level. In our sequenced CD11b$^+$/CD45^{low} cells, we identified seven microglial subtypes as well as small populations of monocytes, macrophages, neutrophils, and neurons. In addition to three homeostatic populations, other microglia subtypes included inflammatory microglia, interferon-related microglia, proliferative microglia, and a cluster with unknown function, which we termed uMG. As far as we are aware, this uMG cluster has not been previously described. It is characterized by upregulation of mitochondrial genes, and perhaps represents a dying subset, as seen in other scRNA-seq data.[49]

We found that diet did not affect the cluster proportions. Homeostatic microglia comprised the largest cell population in all experimental groups. In line with our results, microglial scRNA-seq studies have similarly demonstrated that homeostatic microglia are the largest clusters in both healthy and disease contexts in the adolescent and adult brain.[50–52] The presence of the smaller clusters, InflamMG, IfnMG, ProlifMG, and uMG, is not uniform in the literature, and differs with various factors, including age, brain region, disease state, and study design or perhaps power. We found an InflamMG (*Ccl4/3* expressing) population, which has also been identified in small clusters in the healthy cortex at 2 months and 4 months and as a larger microglial percentage in a model of infectious disease.[52] This inflammatory population, as well as an interferon-related population like our IfnMG cluster (*Ifit3* expressing), are prevalent in the whole brain with aging.[50] A proliferative microglia cluster like our ProlifMG (*Top2a*, *Mki67* expressing) are present in the healthy adult brain,[53] prevalent in the early developing brain[50] and found in the cortex of an HIV infection model.[52] The lack of activated morphology at 1 month aligns with our transcriptomic findings; HFD did not alter the proportion of InflamMG and IfnMG and homeostatic microglia dominated all experimental groups. The apparent trending increase in peripheral immune cell types (monocytes, neutrophils) in HFD versus control samples at 3 months could potentially reflect obesity-induced recruitment of immune cells to the brain.[23]

Our identified populations are unlikely an artifact of processing-associated *ex vivo* activation, because they have been identified with transcriptional inhibition, which we employed, in the roughly 3-month-old mouse brain.[53] Marsh et al. showed that transcriptional inhibition prevented a processing-associated cluster, which has appeared in other microglial scRNA-seq.[53] Overall, we showed, for the first time, that

hippocampal microglia in the healthy adolescent and adult hippocampus are mostly homeostatic microglia, with small populations of inflammatory, proliferative, and interferon-related microglia. Future work is needed to determine whether young age and/or the chronic, low-grade nature of obesity-induced inflammation may have protected against changes in inflammatory microglia proportions, which are seen in microglial scRNA-seq studies in aging[50] and overt transgenic models of disease.[51]

Immune cells function by sensing and responding to their environment, so cell-to-cell communication is an integral part of microglial function.[54] Obesity disrupts the inflammatory milieu in the brain,[23,24] so we asked whether obesity alters intercellular microglial signaling. Thus, we next examined whether diet impacted cell-to-cell interactions in the hippocampus by employing CellChat to infer intercellular communication among microglia. Of the signaling that differed by diet, the pathways driving microglia-to-microglia communication serve a diverse set of biological functions, many implicated in immune modulation of microglia or other immune cell types. These pathways contained glycoproteins with known immunomodulatory roles (e.g., 'HSPG,''ICAM1),[36–39] growth factors (e.g., 'TGFb,' 'PDGF'), and immune antigens (e.g., 'CD86', 'ICOS', 'CD48', and 'VISTA'). Several pathways contained proteins with known pro-inflammatory (*e.g.*, 'HSPG,''IFN-I,''IL6') or anti-inflammatory properties (e.g., 'VISTA,''CD200,''IL6'). Heparan sulfate proteoglycans (HSPGs) are immunomodulators[39] with pro-inflammatory effects on microglia. HSPGs stimulate tumor necrosis factor alpha cytokine production[38] and are involved in the microglial lipopolysaccharide-induced toll-like receptor 4 response.[55] V-domain immunoglobulin-containing suppressor of T cell activation (Vista), plays an immune checkpoint role as a negative regulator of T-cells, and is involved in other myeloid cell functions, such as phagocytosis, but its role in microglia is not well characterized.[56] Both Vista and cell adhesion molecule 1 (*Cadm1*), the ligand and receptor for 'CADM' signaling, are differentially expressed in Alzheimer's disease-associated microglia.[51,56]

Further studies are needed to understand the role of these signaling pathways in modulating microglial behavior in obesity. HFD upregulated more microglial immune and inflammatory signaling at 3 months versus 1 month, which supports the hypothesis that chronic HFD enhances immune responses to obesity. HFD pathways associated with homeostatic and protective microglia (e.g., 'GRN,' 'TGFb,' 'CD200')[40,41,57] might reflect a failed attempt to maintain homeostasis under conditions of stress during obesity. Regarding the involvement of signaling pathways related to adhesion molecules, it is possible to speculate these changes may reflect microglial migration as a component of the inflammatory response. In addition to the interactions identified in this study, it is important to consider that microglia in obesity may interact through ligand-receptor pairs that are not in the CellChat database or with other immune cell types. Moreover, our analysis relied on transcriptomic changes in ligand-receptor expression, which may not necessarily reflect protein expression. However, overall, the changes in intercellular microglia-to-microglia signaling revealed by CellChat suggest microglia respond early to an immune challenge, which ramps up over time, leading to a condition of chronic inflammation.

Next, we examined the effect of HFD on intracellular processes in hippocampal microglia by DEG analyses with KEGG enrichment. DEGs between HFD and control microglia at 1 month were enriched in ribosome and protein processing in the ER KEGG pathways. We identified very few cell cluster specific DEGs, but heat shock proteins related to the protein processing in the ER pathway were dysregulated in HFD homeostatic microglia, particularly at 1 month. There were so few DEGs overall at 3 months that we could not infer much biological pathway significance from KEGG enrichment in HFD versus control microglia. However, at 3 months, complement genes (*C1qa, C1qb*) were upregulated and among the top 20 most significant DEGs in HFD versus control microglia. Many of the DEGs and pathways that were implicated in microglia at 1 month and 3 months overlapped with genes that correlated, either positively or negatively, with progressive body weight gain. These findings encompassed some complement and ribosome genes (positive correlations with body weight), with genes related to protein processing in the ER (negative correlations with body weight). Microglia upregulate C1q in response to insult such as ischemic injury[58] or in a model of Alzheimer's disease.[59] The complement cascade's canonical role is in immune response, but complement is also involved in microglial mediated synaptic pruning in brain development.[60] Hippocampal microglia excessively prune synapses in obesity,[15] so it is possible that complement proteins contribute to this aberrant pruning. In support of this hypothesis, microglia contribute to aberrant complement mediated synaptic pruning in Alzheimer's disease.[59] HFD at 3 months also upregulated genes such as *Trem2*, an Alzheimer's disease associated microglia gene,[51,61] as well as genes encoding enzymes for processing pro-inflammatory arachidonic acid derived mediators, prostaglandins (*Hpgd, Ptgs1*) and leukotrienes (*Ltc4s*).

Microglia DEG fold-changes were low, but relatively consistent with chronic challenge,[62] including chronic HFD.[47] Because there were few total DEGs, we also performed WGNCA on all cells, which identified five gene co-expression modules, four of which differed by diet. KEGG analysis of the brown module, elevated at 1 month in HFD versus control, and the green module, reduced at 3 months in HFD, identified genes enriched in protein processing in the ER. The turquoise module, reduced at 1 month in HFD, was enriched in ribosome genes, and the yellow module, elevated at 1 month and 3 months in HFD versus control, identified genes enriched in Alzheimer's disease and B cell receptor signaling pathways. Overall, DEGs expression in HFD microglia was characterized by an earlier ER response signature at 1 month, followed by a more inflammatory signature at 3 months. These finds align with the correlation analysis of transcript levels with body weight, which was negative for ER response genes, i.e., transcript levels of ER response genes went down with progressive obesity, and positive for complement genes, i.e., transcript levels of complement genes went up with progressive obesity.

Our DEG and WGNCA findings closely align with published bulk RNA-seq data of microglia after 8 weeks of HFD.[47] The study found only 77 DEGs that differed in HFD versus control whole brain microglia and an upregulated WGNCA module containing heat shock protein genes, such as *Hspa8*, *Dnaja1*, *Dnajb1*,[47] which were identified by our study. We also previously found that chronic HFD after 20 weeks induces hippocampal ER stress, enhancing expression of heat shock protein 5 and a member of the canonical inositol requiring enzyme 1 ER stress response, spliced X-box binding protein 1.[63] The link between ER stress and inflammation is a well-studied phenomenon in obesity.[64,65] Saturated fatty acids[66,67] activate the macrophage ER stress response in obesity, which contributes to a pro-inflammatory phenotype.[68] The heat shock proteins upregulated in our study at 1 month, e.g., *Hspa8*, *Dnaja1*, and *Dnajb1*, are protein folding chaperones and co-chaperones, which work to maintain ER homeostasis. Brykczynska et al. proposed that the increase in microglial ER heat shock proteins after 8 weeks HFD might be a protective mechanism.[47] By examining DEGs, we identified an inflammatory gene expression signature later at 3 months, which aligns with enhanced immunomodulatory intercellular microglia-to-microglia driven signaling by CellChat. This inflammatory gene expression signature was characterized by HFD upregulated microglial genes, *e.g.*, *C1qa*, *C1qb*, *Trem2*, *Hpgd*, *Ptgs1*, and *Ltc4s*. Possibly, an early microglial ER heat shock protein response combats increased burden which, if misfolded protein aggregates accumulate, may transition to an ER stress response capable of inducing inflammation.

Additional investigations are required to elucidate the mechanistic underpinnings in the evolving microglial response in obesity, which our findings suggest may be characterized by an earlier ER response, followed by a more chronic inflammatory state. Possibly obesity stressors trigger an adaptive ER response in attempt to maintain homeostatic function at 1 month, which evolves to a more activated state by 3 months. Indeed, rats pretreated with a mild ER stress inducer are protected from lipopolysaccharide-induced cognitive impairment and microglial pro-inflammatory activation, suggesting that mild ER stress may mitigate hippocampal sequela of inflammatory challenge.[69] Alternatively, obesity may trigger a cascade of processes with increased demand on the ER, followed by an injurious ER stress response, which activates inflammatory pathways, as occurs in macrophages in obesity.[68] ER stress has been implicated in microglial mediated inflammation in other disease contexts.[70] Further studies that manipulate microglial ER stress are needed to determine whether it mitigates or contributes to microglial pro-inflammatory activation in obesity. Moreover, our findings indicate potential therapeutic targets for microglia-mediated cognitive impairment secondary to obesity. Targeting complement[59] and prostaglandin[71] in microglia or macrophages slows synapse loss and cognitive decline in aging and Alzheimer's disease models and may, in addition, constitute promising approaches in obesity-induced cognitive impairment.

In summary, we used morphological and scRNA-seq analyses to determine the effects of obesity on hippocampal microglial activation in mice transitioning from adolescence to adulthood. We found that HFD did not alter hippocampal CA1 microglial morphology after just 1 month. We demonstrated, for the first time, the microglial landscape of the healthy adolescent and adult hippocampus in the C57BL/6J mouse. Although diet did not affect cluster proportions, HFD dysregulated intercellular inflammatory signaling pathways, an effect which was more pronounced at 3 months. Analysis of gene expression revealed a microglial signature of dysregulated ER protein processing and ribosome pathways at 1 month, which transitioned into an inflammatory response at 3 months. Identifying these obesity-associated microglial intercellular and intracellular pathways sets the foundation for further studies to elucidate mechanisms of microglial mediated cognitive deficits in obesity.

Limitations of the study

Although our study had several strengths, such as analyzing two time points using a single-cell method to generate granular transcriptomic information in a deeply phenotyped and well characterized model, we also had several weaknesses. First, significant, DEGs exhibited only small fold-changes and varied by lmicroglia cell subtype, making it difficult to validate these findings by bulk analysis of microglial isolations using qPCR. Second, our study only examined transcriptomic changes, and did not provide information on post-transcriptomic differences related to protein expression. Third, the CellChat analysis was limited to microglia interactions that occur through ligand-receptor pairs present in the database. Lastly, our study only included male mice; however, differences in immune system by sex warrant investigation of hippocampal microglia in female HFD versus control mice.[72,73] Future functional studies of an early ER response mediated by hippocampal microglia in HFD mice will be needed to validate these study findings.

STAR★METHODS

Detailed methods are provided in the online version of this paper and include the following:

- KEY RESOURCES TABLE
- RESOURCE AVAILABILITY
  - Lead contact
  - Materials availability
  - Data and code availability
- EXPERIMENTAL MODEL AND SUBJECT DETAILS
- METHOD DETAILS
  - Mouse metabolic phenotyping
  - Microglial isolation, sorting, and scRNA-seq
  - scRNA-seq data alignment and sample aggregating
  - Dimension reduction, clustering, and visualization
  - Celltype annotation and differential expression analysis
  - Cell-to-cell communication
  - Weighted gene co-expression network analysis
  - Correlation analysis of body weights to transcript levels
  - Immunohistochemistry and microglial morphology analysis
- QUANTIFICATION AND STATISTICAL ANALYSIS

SUPPLEMENTAL INFORMATION

Supplemental information can be found online at https://doi.org/10.1016/j.isci.2023.106164.

DECLARATION OF INTERESTS

The authors declare no competing interests.

REFERENCES

1. Obesity and overweight. https://www.who.int/news-room/fact-sheets/detail/obesity-and-overweight.

2. Callaghan, B.C., Reynolds, E.L., Banerjee, M., Chant, E., Villegas-Umana, E., Gardner, T.W., Votruba, K., Giordani, B., Pop-Busui, R., Pennathur, S., and Feldman, E.L. (2020). The prevalence and determinants of cognitive deficits and traditional diabetic complications in the severely obese. Diabetes Care 43, 683–690. https://doi.org/10.2337/dc19-1642.

3. Dekkers, I.A., Jansen, P.R., and Lamb, H.J. (2019). Obesity, brain volume, and white matter microstructure at MRI: a cross-sectional UK biobank study. Radiology 291, 763–771. https://doi.org/10.1148/RADIOL.2019181012.

4. Black, N., Johnston, D.W., and Peeters, A. (2015). Childhood obesity and cognitive achievement. Health Econ. 24, 1082–1100. https://doi.org/10.1002/HEC.3211.

5. Alosco, M.L., Stanek, K.M., Galioto, R., Korgaonkar, M.S., Grieve, S.M., Brickman, A.M., Spitznagel, M.B., and Gunstad, J. (2013). Body mass index and brain structure in healthy children and adolescents. Int. J. Neurosci. 124, 49–55. https://doi.org/10.3109/00207454.2013.817408.

6. Yau, P.L., Castro, M.G., Tagani, A., Tsui, W.H., and Convit, A. (2012). Obesity and metabolic syndrome and functional and structural brain impairments in adolescence. Pediatrics 130, e856–e864. https://doi.org/10.1542/PEDS.2012-0324.

7. Xu, W.L., Atti, A.R., Gatz, M., Pedersen, N.L., Johansson, B., and Fratiglioni, L. (2011). Midlife Overweight and Obesity Increase Late-Life Dementia Risk A Population-Based Twin Study.

8. Pedditzi, E., Peters, R., and Beckett, N. (2016). The risk of overweight/obesity in mid-life and late life for the development of dementia: a systematic review and meta-analysis of longitudinal studies. Age Ageing 45, 14–21. https://doi.org/10.1093/AGEING/AFV151.

9. André, C., Guzman-Quevedo, O., Rey, C., Rémus-Borel, J., Clark, S., Castellanos-Jankiewicz, A., Ladeveze, E., Leste-Lasserre, T., Nadjar, A., Abrous, D.N., et al. (2017). Inhibiting microglia expansion prevents diet-induced hypothalamic and peripheral inflammation. Diabetes 66, 908–919. https://doi.org/10.2337/DB16-0586.

10. Valdearcos, M., Myers, M.G., and Koliwad, S.K. (2019). Hypothalamic microglia as potential regulators of metabolic physiology. Nat. Metab. 1, 314–320. https://doi.org/10.1038/S42255-019-0040-0.

11. Valdearcos, M., Douglass, J.D., Robblee, M.M., Dorfman, M.D., Stifler, D.R., Bennett, M.L., Gerritse, I., Fasnacht, R., Barres, B.A., Thaler, J.P., and Koliwad, S.K. (2017). Microglial inflammatory signaling orchestrates the hypothalamic immune response to dietary excess and mediates obesity susceptibility. Cell Metab. 26, 185–197.e3. https://doi.org/10.1016/J.CMET.2017.05.015.

12. Mendes, N.F., Kim, Y.B., Velloso, L.A., and Araújo, E.P. (2018). Hypothalamic microglial activation in obesity: amini-review. Front. Neurosci. 12, 846. https://doi.org/10.3389/FNINS.2018.00846.

13. Nakandakari, S.C.B.R., Muñoz, V.R., Kuga, G.K., Gaspar, R.C., Sant'Ana, M.R., Pavan, I.C.B., da Silva, L.G.S., Morelli, A.P., Simabuco, F.M., da Silva, A.S.R., et al. (2019). Short-term high-fat diet modulates several inflammatory, ER stress, and apoptosis markers in the hippocampus of young mice. Brain Behav. Immun. 79, 284–293. https://doi.org/10.1016/j.bbi.2019.02.016.

14. Sobesky, J.L., D'Angelo, H.M., Weber, M.D., Anderson, N.D., Frank, M.G., Watkins, L.R., Maier, S.F., and Barrientos, R.M. (2016). Glucocorticoids mediate short-term high-fat diet induction of neuroinflammatory priming, the NLRP3 inflammasome, and the danger signal HMGB1. eNeuro 3. ENEURO.0113-16.2016. https://doi.org/10.1523/ENEURO.0113-16.2016.

15. Cope, E.C., LaMarca, E.A., Monari, P.K., Olson, L.B., Martinez, S., Zych, A.D., Katchur, N.J., and Gould, E. (2018). Microglia play an active role in obesity-associated cognitive decline. J. Neurosci. 38, 8889–8904. https://doi.org/10.1523/JNEUROSCI.0789-18.2018.

16. Hao, S., Dey, A., Yu, X., and Stranahan, A.M. (2016). Dietary obesity reversibly induces synaptic stripping by microglia and impairs hippocampal plasticity. Brain Behav. Immun. 51, 230–239. https://doi.org/10.1016/j.bbi.2015.08.023.

17. Valcarcel-Ares, M.N., Tucsek, Z., Kiss, T., Giles, C.B., Tarantini, S., Yabluchanskiy, A., Balasubramanian, P., Gautam, T., Galvan, V., Ballabh, P., et al. (2019). Obesity in aging exacerbates neuroinflammation, dysregulating synaptic function-related genes and altering eicosanoid synthesis in the mouse Hippocampus: potential role in impaired synaptic plasticity and cognitive decline. J. Gerontol. A Biol. Sci. Med. Sci. 74, 290–298. https://doi.org/10.1093/GERONA/GLY127.

18. Sims-Robinson, C., Bakeman, A., Bruno, E., Jackson, S., Glasser, R., Murphy, G.G., and Feldman, E.L. (2016). Dietary reversal ameliorates short- and long-term memory deficits induced by high-fat diet early in life. PLoS One 11, e0163883. https://doi.org/10.1371/journal.pone.0163883.

19. Guillemot-Legris, O., and Muccioli, G.G. (2017). Obesity-induced neuroinflammation: beyond the hypothalamus. Trends Neurosci. 40, 237–253. https://doi.org/10.1016/J.TINS.2017.02.005.

20. Kang, E.B., Koo, J.H., Jang, Y.C., Yang, C.H., Lee, Y., Cosio-Lima, L.M., and Cho, J.Y. (2016). Neuroprotective effects of endurance exercise against high-fat diet-induced hippocampal neuroinflammation. J. Neuroendocrinol. 28. https://doi.org/10.1111/JNE.12385.

21. Guo, D.H., Yamamoto, M., Hernandez, C.M., Khodadadi, H., Baban, B., and Stranahan, A.M. (2020). Visceral adipose NLRP3 impairs cognition in obesity via IL-1R1 on CX3CR1+ cells. J. Clin. Invest. 130, 1961–1976. https://doi.org/10.1172/JCI126078.

22. Melo, H.M., Seixas da Silva, G.d.S., Sant'Ana, M.R., Teixeira, C.V.L., Clarke, J.R., Miya Coreixas, V.S., de Melo, B.C., Fortuna, J.T.S., Forny-Germano, L., Ledo, J.H., et al. (2020). Palmitate is increased in the cerebrospinal fluid of humans with obesity and induces memory impairment in mice via pro-inflammatory TNF-α. Cell Rep. 30, 2180–2194.e8. https://doi.org/10.1016/j.celrep.2020.01.072.

23. Buckman, L.B., Hasty, A.H., Flaherty, D.K., Buckman, C.T., Thompson, M.M., Matlock, B.K., Weller, K., and Ellacott, K.L.J. (2014). Obesity induced by a high-fat diet is associated with increased immune cell entry into the central nervous system. Brain Behav. Immun. 35, 33–42. https://doi.org/10.1016/J.BBI.2013.06.007.

24. Salas-Venegas, V., Flores-Torres, R.P., Rodríguez-Cortés, Y.M., Rodríguez-Retana, D., Ramírez-Carreto, R.J., Concepción-Carrillo, L.E., Pérez-Flores, L.J., Alarcón-Aguilar, A., López-Díazguerrero, N.E., Gómez-González, B., et al. (2022). The obese brain: mechanisms of systemic and local inflammation, and interventions to reverse the cognitive deficit. Front. Integr. Neurosci. 16, 798995. https://doi.org/10.3389/FNINT.2022.798995.

25. Valdearcos, M., Robblee, M.M., Benjamin, D.I., Nomura, D.K., Xu, A.W., and Koliwad, S.K. (2014). Microglia dictate the impact of saturated fat consumption on hypothalamic inflammation and neuronal function. Cell Rep. 9, 2124–2138. https://doi.org/10.1016/j.celrep.2014.11.018.

26. Sims-Robinson, C., Zhao, S., Hur, J., and Feldman, E.L. (2012). Central nervous system endoplasmic reticulum stress in a murine model of type 2 diabetes. Diabetologia 55, 2276–2284. https://doi.org/10.1007/s00125-012-2573-6.

27. Eid, S.A., and Feldman, E.L. (2021). Advances in diet-induced rodent models of metabolically acquired peripheral neuropathy. Dis. Model. Mech. 14, dmm049337. https://doi.org/10.1242/DMM.049337.

28. de Moura e Dias, M., dos Reis, S.A., da Conceição, L.L., Sediyama, C.M.N.d.O., Pereira, S.S., de Oliveira, L.L., Gouveia Peluzio, M.d.C., Martinez, J.A., and Milagro, F.I. (2021). Diet-induced obesity in animal models: points to consider and influence on metabolic markers. Diabetol. Metab. Syndr. 13, 32. https://doi.org/10.1186/S13098-021-00647-2.

29. O'Brien, P.D., Hinder, L.M., Rumora, A.E., Hayes, J.M., Dauch, J.R., Backus, C., Mendelson, F.E., and Feldman, E.L. (2018). Juvenile murine models of prediabetes and type 2 diabetes develop neuropathy. Dis. Model. Mech. 11, dmm037374. https://doi.org/10.1242/dmm.037374.

30. York, E.M., Ledue, J.M., Bernier, L.P., and Macvicar, B.A. (2018). 3dmorph automatic analysis of microglial morphology in three dimensions from ex vivo and in vivo imaging. eNeuro 5. ENEURO.0266-18.2018. https://doi.org/10.1523/ENEURO.0266-18.2018.

31. Colonna, M., and Butovsky, O. (2017). Microglia function in the central nervous system during Health and neurodegeneration. Annu. Rev. Immunol. 35, 441–468. https://doi.org/10.1146/ANNUREV-IMMUNOL-051116-052358.

32. ElAli, A., and Rivest, S. (2016). Microglia ontology and signaling. Front. Cell Dev. Biol. 4, 72. https://doi.org/10.3389/fcell.2016.00072.

33. Nimmerjahn, A., Kirchhoff, F., and Helmchen, F. (2005). Resting microglial cells are highly dynamic surveillants of brain parenchyma in vivo. Science 308, 1314–1318. https://doi.org/10.1126/SCIENCE.1110647.

34. Jin, S., Guerrero-Juarez, C.F., Zhang, L., Chang, I., Ramos, R., Kuan, C.-H., Myung, P., Plikus, M.V., and Nie, Q. (2021). Inference and analysis of cell-cell communication using CellChat. Nat. Commun. 12, 1088. https://doi.org/10.1038/s41467-021-21246-9.

35. Wimmer, I., Tietz, S., Nishihara, H., Deutsch, U., Sallusto, F., Gosselet, F., Lyck, R., Muller, W.A., Lassmann, H., and Engelhardt, B. (2019). PECAM-1 stabilizes blood-brain barrier integrity and favors paracellular T-cell diapedesis across the blood-brain barrier during neuroinflammation. Front. Immunol.

10, 711. https://doi.org/10.3389/FIMMU.2019.00711.

36. Van De Stolpe, A., and Van Der Saag, P.T. (1996). Intercellular adhesion molecule-1. J. Mol. Med. 74, 13–33. https://doi.org/10.1007/BF00202069.

37. Werner, A., Kloss, C.U., Walter, J., Kreutzberg, G.W., and Raivich, G. (1998). Intercellular adhesion molecule-1 (ICAM-1) in the mouse facial motor nucleus after axonal injury and during regeneration. J. Neurocytol. 27, 219–232. https://doi.org/10.1023/A:1006928830251.

38. Bussini, S., Meda, L., Scarpini, E., Clementi, E., Conti, G., Tiriticco, M., Bresolin, N., and Baron, P. (2005). Heparan sulfate proteoglycan induces the production of NO and TNF-α by murine microglia. Immun. Ageing 2, 11. https://doi.org/10.1186/1742-4933-2-11.

39. O'Callaghan, P., Zhang, X., and Li, J.P. (2018). Heparan sulfate proteoglycans as relays of neuroinflammation. J. Histochem. Cytochem. 66, 305–319. https://doi.org/10.1369/0022155417742147.

40. Lyons, A., Downer, E.J., Crotty, S., Nolan, Y.M., Mills, K.H.G., and Lynch, M.A. (2007). CD200 ligand–receptor interaction modulates microglial activation in vivo and in vitro: arole for IL-4. J. Neurosci. 27, 8309–8313. https://doi.org/10.1523/JNEUROSCI.1781-07.2007.

41. Telpoukhovskaia, M.A., Liu, K., Sayed, F.A., Etchegaray, J.I., Xie, M., Zhan, L., Li, Y., Zhou, Y., Le, D., Bahr, B.A., et al. (2020). Discovery of small molecules that normalize the transcriptome and enhance cysteine cathepsin activity in progranulin-deficient microglia. Sci. Rep. 10, 13688. https://doi.org/10.1038/s41598-020-70534-9.

42. Rhinn, H., Tatton, N., McCaughey, S., Kurnellas, M., and Rosenthal, A. (2022). Progranulin as a therapeutic target in neurodegenerative diseases. Trends Pharmacol. Sci. 43, 641–652. https://doi.org/10.1016/J.TIPS.2021.11.015.

43. Rünker, A.E., Little, G.E., Suto, F., Fujisawa, H., and Mitchell, K.J. (2008). Semaphorin-6A controls guidance of corticospinal tract axons at multiple choice points. Neural Dev. 3, 1–19. https://doi.org/10.1186/1749-8104-3-34.

44. Rothaug, M., Becker-Pauly, C., and Rose-John, S. (2016). The role of interleukin-6 signaling in nervous tissue. Biochim. Biophys. Acta 1863, 1218–1227. https://doi.org/10.1016/J.BBAMCR.2016.03.018.

45. Andrae, J., Gallini, R., and Betsholtz, C. (2008). Role of platelet-derived growth factors in physiology and medicine. Genes Dev. 22, 1276–1312. https://doi.org/10.1101/GAD.1653708.

46. Pierce, G.F., Mustoe, T.A., Altrock, B.W., Deuel, T.F., and Thomason, A. (1991). Role of platelet-derived growth factor in wound healing. J. Cell. Biochem. 45, 319–326. https://doi.org/10.1002/JCB.240450403.

47. Brykczynska, U., Geigges, M., Wiedemann, S.J., Dror, E., Böni-Schnetzler, M., Hess, C., Donath, M.Y., and Paro, R. (2020). Distinct transcriptional responses across tissue-resident macrophages to short-term and long-term metabolic challenge. Cell Rep. 30, 1627–1643.e7. https://doi.org/10.1016/J.CELREP.2020.01.005.

48. Tarantini, S., Valcarcel-Ares, M.N., Yabluchanskiy, A., Tucsek, Z., Hertelendy, P., Kiss, T., Gautam, T., Zhang, X.A., Sonntag, W.E., de Cabo, R., et al. (2018). Nrf2 deficiency exacerbates obesity-induced oxidative stress, neurovascular dysfunction, blood-brain barrier disruption, neuroinflammation, amyloidogenic gene expression, and cognitive decline in mice, mimicking the aging phenotype. J. Gerontol. A Biol. Sci. Med. Sci. 73, 853–863. https://doi.org/10.1093/GERONA/GLX177.

49. Braeuer, R.R., Walker, N.M., Misumi, K., Mazzoni-Putman, S., Aoki, Y., Liao, R., Vittal, R., Kleer, G.G., Wheeler, D.S., Sexton, J.Z., et al. (2021). Transcription factor FOXF1 identifies compartmentally distinct mesenchymal cells with a role in lung allograft fibrogenesis. J. Clin. Invest. 131, e147343. https://doi.org/10.1172/JCI147343.

50. Hammond, T.R., Dufort, C., Dissing-Olesen, L., Giera, S., Young, A., Wysoker, A., Walker, A.J., Gergits, F., Segel, M., Nemesh, J., et al. (2019). Single-cell RNA sequencing of microglia throughout the mouse lifespan and in the injured brain reveals complex cell-state changes. Immunity 50, 253–271.e6. https://doi.org/10.1016/j.immuni.2018.11.004.

51. Keren-Shaul, H., Spinrad, A., Weiner, A., Matcovitch-Natan, O., Dvir-Szternfeld, R., Ulland, T.K., David, E., Baruch, K., Lara-Astaiso, D., Toth, B., et al. (2017). A unique microglia type associated with restricting development of Alzheimer's disease. Cell 169, 1276–1290.e17. https://doi.org/10.1016/j.cell.2017.05.018.

52. Zheng, J., Ru, W., Adolacion, J.R., Spurgat, M.S., Liu, X., Yuan, S., Liang, R.X., Dong, J., Potter, A.S., Potter, S.S., et al. (2021). Single-cell RNA-seq analysis reveals compartment-specific heterogeneity and plasticity of microglia. iScience 24, 102186. https://doi.org/10.1016/J.ISCI.2021.102186.

53. Marsh, S.E., Walker, A.J., Kamath, T., Dissing-Olesen, L., Hammond, T.R., de Soysa, T.Y., Young, A.M.H., Murphy, S., Abdulraouf, A., Nadaf, N., et al. (2022). Dissection of artifactual and confounding glial signatures by single-cell sequencing of mouse and human brain. Nat. Neurosci. 25, 306–316. https://doi.org/10.1038/s41593-022-01022-8.

54. Borst, K., Dumas, A.A., and Prinz, M. (2021). Microglia: immune and non-immune functions. Immunity 54, 2194–2208. https://doi.org/10.1016/J.IMMUNI.2021.09.014.

55. O'Callaghan, P., Li, J.P., Lannfelt, L., Lindahl, U., and Zhang, X. (2015). Microglial heparan sulfate proteoglycans facilitate the cluster-of-differentiation 14 (CD14)/Toll-like receptor 4 (TLR4)-Dependent inflammatory response. J. Biol. Chem. 290, 14904–14914. https://doi.org/10.1074/JBC.M114.634337.

56. Borggrewe, M., Kooistra, S.M., Noelle, R.J., Eggen, B.J.L., and Laman, J.D. (2020). Exploring the VISTA of microglia: immune checkpoints in CNS inflammation. J. Mol. Med. *98*, 1415–1430. https://doi.org/10.1007/S00109-020-01968-X.

57. Zöller, T., Schneider, A., Kleimeyer, C., Masuda, T., Potru, P.S., Pfeifer, D., Blank, T., Prinz, M., and Spittau, B. (2018). Silencing of TGFβ signalling in microglia results in impaired homeostasis. Nat. Commun. *9*, 4011. https://doi.org/10.1038/s41467-018-06224-y.

58. Schäfer, M.K., Schwaeble, W.J., Post, C., Salvati, P., Calabresi, M., Sim, R.B., Petry, F., Loos, M., and Weihe, E. (2000). Complement C1q is dramatically up-regulated in brain microglia in response to transient global cerebral ischemia. J. Immunol. *164*, 5446–5452. https://doi.org/10.4049/JIMMUNOL.164.10.5446.

59. Hong, S., Beja-Glasser, V.F., Nfonoyim, B.M., Frouin, A., Li, S., Ramakrishnan, S., Merry, K.M., Shi, Q., Rosenthal, A., Barres, B.A., et al. (2016). Complement and microglia mediate early synapse loss in Alzheimer mouse models. Science *352*, 712–716. https://doi.org/10.1126/SCIENCE.AAD8373.

60. Schartz, N.D., and Tenner, A.J. (2020). The good, the bad, and the opportunities of the complement system in neurodegenerative disease. J. Neuroinflammation *17*, 354. https://doi.org/10.1186/S12974-020-02024-8.

61. McQuade, A., Kang, Y.J., Hasselmann, J., Jairaman, A., Sotelo, A., Coburn, M., Shabestari, S.K., Chadarevian, J.P., Fote, G., Tu, C.H., et al. (2020). Gene expression and functional deficits underlie TREM2-knockout microglia responses in human models of Alzheimer's disease. Nat. Commun. *11*, 5370. https://doi.org/10.1038/s41467-020-19227-5.

62. McCarthy, G.M., Farris, S.P., Blednov, Y.A., Harris, R.A., and Mayfield, R.D. (2018). Microglial-specific transcriptome changes following chronic alcohol consumption. Neuropharmacology *128*, 416–424. https://doi.org/10.1016/J.NEUROPHARM.2017.10.035.

63. Sims-Robinson, C., Bakeman, A., Glasser, R., Boggs, J., Pacut, C., and Feldman, E.L. (2016). The role of endoplasmic reticulum stress in hippocampal insulin resistance. Exp. Neurol. *277*, 261–267. https://doi.org/10.1016/j.expneurol.2016.01.007.

64. Hummasti, S., and Hotamisligil, G.S. (2010). Endoplasmic reticulum stress and inflammation in obesity and diabetes. Circ. Res. *107*, 579–591. https://doi.org/10.1161/CIRCRESAHA.110.225698.

65. Hotamisligil, G.S. (2010). Endoplasmic reticulum stress and the inflammatory basis of metabolic disease. Cell *140*, 900–917. https://doi.org/10.1016/J.CELL.2010.02.034.

66. Korbecki, J., and Bajdak-Rusinek, K. (2019). The effect of palmitic acid on inflammatory response in macrophages: an overview of molecular mechanisms. Inflamm. Res. *68*, 915–932. https://doi.org/10.1007/S00011-019-01273-5.

67. Robblee, M.M., Kim, C.C., Porter Abate, J., Valdearcos, M., Sandlund, K.L.M., Shenoy, M.K., Volmer, R., Iwawaki, T., and Koliwad, S.K. (2016). Saturated fatty acids engage an IRE1α-dependent pathway to activate the NLRP3 inflammasome in myeloid cells. Cell Rep. *14*, 2611–2623. https://doi.org/10.1016/j.celrep.2016.02.053.

68. Shan, B., Wang, X., Wu, Y., Xu, C., Xia, Z., Dai, J., Shao, M., Zhao, F., He, S., Yang, L., et al. (2017). The metabolic ER stress sensor IRE1α suppresses alternative activation of macrophages and impairs energy expenditure in obesity. Nat. Immunol. *18*, 519–529. https://doi.org/10.1038/ni.3709.

69. Wang, Y., Zhou, Q., Zhang, X., Qian, Q., Xu, J., Ni, P., and Qian, Y. (2017). Mild endoplasmic reticulum stress ameliorates lipopolysaccharide-induced neuroinflammation and cognitive impairment via regulation of microglial polarization. J. Neuroinflammation *14*, 233. https://doi.org/10.1186/s12974-017-1002-7.

70. Shi, M., Chai, Y., Zhang, J., and Chen, X. (2022). Endoplasmic reticulum stress-associated neuronal death and innate immune response in neurological diseases. Front. Immunol. *12*, 5796. https://doi.org/10.3389/FIMMU.2021.794580.

71. Minhas, P.S., Latif-Hernandez, A., McReynolds, M.R., Durairaj, A.S., Wang, Q., Rubin, A., Joshi, A.U., He, J.Q., Gauba, E., Liu, L., et al. (2021). Restoring metabolism of myeloid cells reverses cognitive decline in ageing. Nature *590*, 122–128. https://doi.org/10.1038/S41586-020-03160-0.

72. Nelson, L.H., and Lenz, K.M. (2017). The immune system as a novel regulator of sex differences in brain and behavioral development. J. Neurosci. Res. *95*, 447–461. https://doi.org/10.1002/JNR.23821.

73. Gubbels Bupp, M.R. (2015). Sex, the aging immune system, and chronic disease. Cell. Immunol. *294*, 102–110. https://doi.org/10.1016/J.CELLIMM.2015.02.002.

74. Franzén, O., Gan, L.M., and Björkegren, J.L.M. (2019). PanglaoDB: a web server for exploration of mouse and human single-cell RNA sequencing data. Database *2019*, baz046. https://doi.org/10.1093/DATABASE/BAZ046.

75. Zhang, X., Lan, Y., Xu, J., Quan, F., Zhao, E., Deng, C., Luo, T., Xu, L., Liao, G., Yan, M., et al. (2019). CellMarker: a manually curated resource of cell markers in human and mouse. Nucleic Acids Res. *47*, D721–D728. https://doi.org/10.1093/NAR/GKY900.

76. Stuart, T., Butler, A., Hoffman, P., Hafemeister, C., Papalexi, E., Mauck, W.M., Hao, Y., Stoeckius, M., Smibert, P., R, S., and Satija, R. (2019). Comprehensive integration of single-cell data. Cell *177*, 1888–1902.e21. https://doi.org/10.1016/J.CELL.2019.05.031.

77. Love, M.I., Huber, W., and Anders, S. (2014). Moderated estimation of fold change and dispersion for RNA-seq data with DESeq2. Genome Biol. *15*, 550. https://doi.org/10.1186/S13059-014-0550-8.

78. Aibar, S., González-Blas, C.B., Moerman, T., Huynh-Thu, V.A., Imrichova, H., Hulselmans, G., Rambow, F., Marine, J.C., Geurts, P., Aerts, J., et al. (2017). SCENIC: single-cell regulatory network inference and clustering. Nat. Methods *14*, 1083–1086. https://doi.org/10.1038/nmeth.4463.

79. Huynh-Thu, V.A., Irrthum, A., Wehenkel, L., and Geurts, P. (2010). Inferring regulatory networks from expression data using tree-based methods. PLoS One *5*, e12776. https://doi.org/10.1371/journal.pone.0012776.

80. Trapnell, C., Cacchiarelli, D., Grimsby, J., Pokharel, P., Li, S., Morse, M., Lennon, N.J., Livak, K.J., Mikkelsen, T.S., and Rinn, J.L. (2014). The dynamics and regulators of cell fate decisions are revealed by pseudotemporal ordering of single cells. Nat. Biotechnol. *32*, 381–386. https://doi.org/10.1038/nbt.2859.

81. Zheng, G.X.Y., Terry, J.M., Belgrader, P., Ryvkin, P., Bent, Z.W., Wilson, R., Ziraldo, S.B., Wheeler, T.D., McDermott, G.P., Zhu, J., et al. (2017). Massively parallel digital transcriptional profiling of single cells. Nat. Commun. *8*, 14049. https://doi.org/10.1038/NCOMMS14049.

82. Stoeckius, M., Zheng, S., Houck-Loomis, B., Hao, S., Yeung, B.Z., Mauck, W.M., Smibert, P., and Satija, R. (2018). Cell Hashing with barcoded antibodies enables multiplexing and doublet detection for single cell genomics. Genome Biol. *19*, 224. https://doi.org/10.1186/S13059-018-1603-1.

83. Nikodemova, M., Kimyon, R.S., De, I., Small, A.L., Collier, L.S., and Watters, J.J. (2015). Microglial numbers attain adult levels after undergoing a rapid decrease in cell number in the third postnatal week. J. Neuroimmunol. *278*, 280–288. https://doi.org/10.1016/J.JNEUROIM.2014.11.018.

84. Tay, T.L., Savage, J.C., Hui, C.W., Bisht, K., and Tremblay, M.È. (2017). Microglia across the lifespan: from origin to function in brain development, plasticity and cognition. J. Physiol. *595*, 1929–1945. https://doi.org/10.1113/JP272134.

85. Zhang, B., and Horvath, S. (2005). A general framework for weighted gene co-expression network analysis. Stat. Appl. Genet. Mol. Biol. *4*, Article17. https://doi.org/10.2202/1544-6115.1128.

86. Kuznetsova, A., Brockhoff, P.B., and Christensen, R.H.B. (2017). lmerTest package: tests in linear mixed effects models. J. Stat. Softw. *82*, 1–26. https://doi.org/10.18637/JSS.V082.I13.

STAR★METHODS

KEY RESOURCES TABLE

REAGENT or RESOURCE	SOURCE	IDENTIFIER
Antibodies		
TruStain FcX™ (Anti-Mouse CD16/32)	Biolegend	Cat#101320; RRID: AB_1574975
Rat APC anti-mouse CD45	Biolegend	Cat#103111; RRID: AB_312976
Rat APC-Cy7 anti-mouse/human CD11b	Biolegend	Cat#101226; RRID: AB_830642
TotalSeq™-B0301 Anti-Mouse Hashtag 1 Antibody	BioLegend	Cat#155831; RRID: AB_2814067
TotalSeq™-B0302 Anti-Mouse Hashtag 2 Antibody	BioLegend	Cat#155833; RRID: AB_2814068
TotalSeq™-B0303 Anti-Mouse Hashtag 3 Antibody	BioLegend	Cat#155835; RRID: AB_2814069
Rabbit Anti-IBA1	Wako	Cat#019-19741; RRID: AB_839504
Goat-Anti Rabbit Alexa-Fluor Plus 594	Invitrogen, Thermo Fisher Scientific	Cat#A32740; RRID: AB_2762824
Chemicals, peptides, and recombinant proteins		
Glucose	Sigma-Aldrich, Merck	Cat#G8270-1KG
Intraperitoneal Pentobarbitol (Fatal-Plus)	Vortech	Cat#NDC0298-9373-68
Hanks Phosphate Buffered Saline (no Calcium, no Magnesium, no Phenol Red)	Gibco, Thermo Fisher Scientific	Cat#14175145
Hanks Phosphate Buffered Saline(10X) (no Calcium, no Magnesium, no Phenol Red)	Gibco, Thermo Fisher Scientific	Cat#14185052
Hanks Buffered Phosphate Saline (Calcium, Magnesium, no Phenol Red)	Gibco, Thermo Fisher Scientific	Cat#14025092
Hoechst 33258 Nuclear Stain	Sigma-Aldrich, Merck	Cat#861405
Triptolide	Sigma-Aldrich, Merck	Cat#T3652
Triptolide	Cayman Chemical	Cat#11973
Anisomycin	Sigma-Aldrich, Merck	Cat#A9789
Hibernate A-Calcium-Magnesium	BrainBits	Cat#HACAMG
Glutamax	Gibco, Thermo Fisher Scientific	Cat#35050061
Papain	Worthington	Cat#LS003119
Transcription Inhibitors Actinomycin D	Sigma-Aldrich, Merck	Cat#A1410
Percoll	Cytiva	Cat#17089102
10XPhosphate-Buffered Saline	Thermo Fisher Scientific	Cat#70011044
2% Fetal Bovine Serum	Corning	Cat#35-011-CV
Ethylenediaminetetraacetic Acid	Sigma-Aldrich, Merck	Cat#E7889
Sucrose	Sigma-Aldrich, Merck	Cat#84097-5KG
Paraformaldehyde	Sigma-Aldrich, Merck	Cat#P6148-500G
Critical commercial assays		
KAPA Library Quantification Kit	Roche	Cat#07960140001
Deposited data		
scRNA-seq data collected in this study	GEO	NCBI Gene Expression Omnibus, accession ID GSE217464
Data analysis codes for this study	Github	https://github.com/hurlab/HF_iScience
PanglaoDB: a web server for exploration of mouse and human single-cell RNA sequencing data	Panglao DB	Franzén et al.[74]
CellMarker	CellMarker	Zhang et al.[75]
Kyoto Encyclopedia of Genes and Genomes	Kanehisa Laboratories	https://www.genome.jp/kegg/

(Continued on next page)

Continued

REAGENT or RESOURCE	SOURCE	IDENTIFIER
Experimental models: Organisms/strains		
C57BL/6J Mice	Jackson Laboratory, Bar Harbor, ME, USA	Cat#000664; RRID:IMSR_JAX:000664
Software and algorithms		
Bcl2fastq2 Conversion Software	Illumina	https://emea.support.illumina.com/downloads/bcl2fastq-conversion-software-v2-20.html
CellRanger Pipeline v4.0	10x Genomics	https://support.10xgenomics.com/single-cell-gene-expression/software/pipelines/latest/what-is-cell-ranger
Seurat v3	Stuart et al.[76]	https://satijalab.org/seurat/install.html
Uniform Manifold Approximation and Projection (UMAP)	Seurat	https://satijalab.org/seurat/reference/runumap
DESeq2 version 1.24.0	Love et al.[77]	https://bioconductor.org/packages/release/bioc/html/DESeq2.html
richR	Open Source	https://github.com/hurlab/richR
CellChat	Jin et al.[34]	http://www.cellchat.org/
WGCNA R package	CRAN	https://cran.r-project.org/web/packages/WGCNA/index.html
sva R package	Bioconductor	https://bioconductor.org/packages/release/bioc/html/sva.html
Imaris Software	Oxford Instruments	https://imaris.oxinst.com/products/imaris-for-cell-biologists?gclid=CjwKCAjwuYWSBhByEiwAKd_n_u39sLI-SVsq6RZTWcYMNDDJFUGacHiJfNo-dOjoTHFHVeNLplaNHBoCIo4QAvD_BwE
3DMorph Script	MATLAB, Elisa M York	https://github.com/ElisaYork/3DMorph
Prism 9	Graph Pad by Dotmatics	https://www.graphpad.com/scientific-software/prism/
lmerTest R package v4.1.1	CRAN	https://cran.r-project.org/web/packages/lmerTest/lmerTest.pdf
SCENIC	Aibar et al.[78]	https://scenic.aertslab.org/
GENIE3	Huynh-Thu et al.[79]	https://bioconductor.org/packages/release/bioc/html/GENIE3.html
AUCell	Aibar et al.[78]	https://github.com/aertslab/AUCell
Discriminant Regulon Expression Analysis (DoRothEA) R package	Bioconductor	https://bioconductor.org/packages/release/data/experiment/html/dorothea.html
pheatmap R package	CRAN	https://cran.r-project.org/web/packages/pheatmap/index.htm
ggplot2 R package	CRAN	https://cran.r-project.org/web/packages/ggplot2/index.html
TranscripTools R package	rdrr.io	https://rdrr.io/github/abc-igmm/transcripTools/
Monocle	Trapnell et al.[80]	http://cole-trapnell-lab.github.io/monocle-release/
Other		
Control Diet:10% Fat, 70% Carbohydrates, 20% Protein	Research Diets	Cat#D12450J
HFD (High-Fat Diet): 60% Fat, 20% Carbohydrates, 20% Protein	Research Diets	Cat#D12492

(Continued on next page)

Continued

REAGENT or RESOURCE	SOURCE	IDENTIFIER
Glucometers	AlphaTrak, Abbott Laboratories	Cat#ART12303
Blood Glucose Test Stripes	AlphaTrak, Abbott Laboratories	Cat#71681-01
Sterile .5mm Silanized Glass Pasteur Pipette	BrainBits	Cat#NC0319875
70μm Nylon Cell Strainer	Falcon	Cat#352350
MA900 Multi-Application Cell Sorter	Sony	Ma900
Countess II Automated Cell Counter	Thermo Fisher Scientific	Cat#AMQAX1000
Chromium Next GEM Chip G	10X Genomics	Cat#2000177
Chromium Controller	10X Genomics	Cat#PN-120223;120246
Tapestation 4200	Agilent	Cat#G2991AA
NovaSeq 6000	Illumina	Cat#20013850
Leica Stellaris 8 Falcon Confocal Microscope	Leica	https://www.leica-microsystems.com/ppc/confocal/na/confocal-reimagined/?nlc=20211206-SFDC-013738&utm_source=google&utm_medium=cpc&utm_campaign=Confocal_Stellaris_Generic&utm_content=text_ad&utm_term=confocal%20microscopy&gclid=Cj0KCQjw0PWRBhDKARIsAPKHFGhlshKjfHERcztyilMGquhOJWVh_dLX-vbhDkiVvysxcnuhOYqhugIaAgOPEALw_wcB

RESOURCE AVAILABILITY

Lead contact

Requests for or questions about resources or reagents can be directed to the lead contact, Eva L. Feldman (efeldman@med.umich.edu).

Materials availability

This study did not generate new materials.

Data and code availability

scRNA-seq data generated from this study has been deposited into the NCBI Gene Expression Omnibus with accession ID GSE217464. The data analysis codes can be found at: https://github.com/hurlab/HF_iScience. Any additional information required to reanalyze the data reported in this paper is available from the lead contact upon request.

EXPERIMENTAL MODEL AND SUBJECT DETAILS

The HFD model is an established and deeply phenotyped mouse model of diet-induced obesity,[27,28] which we have previously used in our studies.[29] Male C57BL/6J mice were obtained (Jackson Laboratory, catalog # 000664) at 4 weeks (wk) of age (n=40) and housed in a specific-pathogen-free facility at the Unit for Laboratory Animal Medicine (ULAM) at the University of Michigan. Mice were housed in cages with littermates on paper bedding at $20 \pm 2°C$ and a 12/12-h light/dark cycle and were monitored daily by ULAM staff. Mice were acclimated for 1 wk, and at 5 wk of age were randomized to four groups: Control 1 month (mo) and 3 mo and HFD 1 mo and 3 mo (Figure 1A). Control diet (10% fat, 70% carbohydrates, 20% protein; Research Diets, catalog #D12450J) or HFD (60% fat, 20% carbohydrates, 20% protein; Research Diets, catalog #D12492) were provided *ad libitum*, and mice also had free access to water. All procedures were performed according to a protocol approved by the University of Michigan's Institutional Animal Care and Use Committee (IACUC; PRO00008116, approved 2 May 2018).

METHOD DETAILS

Mouse metabolic phenotyping

HFD and control mice were weighed weekly, except at weeks 6 and 9. Baseline glucose tolerance tests (GTTs) were performed for all animals at 5 wk of age. 1 mo control and HFD mice had GTTs at the 1 mo endpoint; 3 mo control and HFD mice had GTTs at both 1 mo and 3 mo endpoints. For GTTs, mice were fasted for 4 hours (h), and blood glucose levels were measured from one drop of tail blood using a glucometer (AlphaTrak, Abbott Laboratories) at baseline and at 15, 30, 60, and 120 minutes (min) after intraperitoneal injection of 1 g/kg body mass glucose in normal saline. Additional metabolic phenotyping included terminal plasma insulin, cholesterol, triglycerides, phospholipids, and non-esterified fatty acids performed by the Mouse Metabolic Phenotyping Center at the University of Cincinnati.

Microglial isolation, sorting, and scRNA-seq

Mice were euthanized using an IACUC approved protocol. Mice were injected with intraperitoneal pentobarbital (Fatal-Plus, Vortech Pharmaceuticals) and perfused with Hanks' balanced salt solution (HBSS; Thermo Fisher, catalog # 14175-145) supplemented with the transcription inhibitors actinomycin D (5 µg/ml; Sigma, catalog # A1410) and triptolide (10 µM; Sigma, catalog #T3652 or Cayman Chemical #11973), an approach described by Marsh et al.[53] All subsequent microglial isolation steps were performed on ice or at 4°C when possible and in a laminar flow hood or biological safety cabinet. Transcription inhibitors and ice were used to minimize processing-associated microglial activation to preserve an in vivo transcriptional state. Hippocampi were dissected from HFD and control mice (n=6 per group) and minced on ice. A single cell suspension was prepared by a papain enzymatic digestion at 37°C followed by trituration (1 mg/ml; Worthington catalog # LS003119) in Hibernate A-Calcium-Magnesium (BrainBits, catalog # HACAMG) media with Glutamax (~0.5 nM; Gibco, catalog # 35050061). Transcription inhibitors actinomycin D, triptolide, and anisomycin (27.1 µg/ml; Sigma, catalog # A9789) were used until the end of the enzymatic digestion step.

Digested tissue was serially triturated at room temperature with a fire-polished pipette twice followed by a smaller diameter salinized ~0.5 mm fire polished pipette twice (BrainBits, catalog # FPP). The cell suspension was passed through a wet 70 µm strainer on ice and then pelleted. Microglia were enriched by resuspending in 40% Percoll and centrifuging at 500g for 30min at room temperature. The cell pellet was washed in ice-cold HBSS, centrifuged for 10min at 300g at 4°C, and resuspended in ice-cold flow sorting buffer (1X PBS [phosphate buffered saline], 2% fetal bovine serum, 1 mM ethylenediaminetetraacetic acid). Cells were moved to a 96-well plate, blocked with TruStain FcX™ (anti-mouse CD16/32) (Biolegend, catalog # 101320) for 30 min on ice, and then incubated with APC-CD45 (Biolegend, catalog # 103112) and APC-Cy7-CD11b (Biolegend, catalog # 101226) at 1:50 in the presence of 1 µg/100 µl TotalSeq-B anti-mouse Hashtag antibodies (Biolegend, catalog #s 155831, 155833, 155835) for 30 min on ice.

After staining, cells were washed with 200 µl ice-cold flow sorting buffer for 10min at 4°C and resuspended for flow sorting on the Sony MA900 Cell Sorter by the University of Michigan Flow Cytometry Core. The FACS sorting strategy first sorted cells by froward and side scatter, to exclude mostly dead or dying cells along with cellular debris. Gating then selected cells that were CD45^{low} and CD11b^{+}. Tagged control and HFD samples were combined on 10X chips to mitigate batch effects. scRNA-seq was performed by the Advanced Genomics Core at the University of Michigan using the 10X Genomics Chromium system (10X Genomics): An automated counter (Countess II, Thermo Fisher) was used to quantify cells/µl. The single cell suspension was then diluted to a final concentration ranging from 700 to 1000 cells/µl. Using the Chromium Controller, 3' libraries of single cells were created leveraging 3' V3.1 chemistry using NextGEM Chip G reagents, according to the manufacturer's protocol (all from 10X Genomics). The quality of the final library was evaluated by Tapestation 4200 (Agilent) and Kapa qPCR (Roche) was used to quantify libraries. Pooled libraries were sequenced using 150 bp paired-end format (Illumina NovaSeq 6000). De-multiplexed Fastq files were generated (Bcl2fastq2 Conversion Software, Illumina) and reads were aligned and counted (CellRanger Pipeline, 10X Genomics).

scRNA-seq data alignment and sample aggregating

Raw data from 4,644 (HFD 1 mo), 5,024 (control 1 mo), 1,366 (HFD 3 mo), and 1,314 (control 3 mo) cells were obtained from sequencing. Low-quality reads were filtered out (quality less than Q30) and reads were then mapped to the GRCm38 mouse reference genome (CellRanger Pipeline[81] version 4.0.0, 10X Genomics).

The individual sample output files from CellRanger Count were read into Seurat v3.[76] The hashtag oligo (HTO)[82] raw counts of each cell were normalized using a centered log ratio transformation across cells. Cells were then demultiplexed by using the HTODemux function in Seurat,[76] and droplets with two cells (doublets), more than two cells, or no cell (empty droplet) were subsequently removed. Cells were excluded from downstream analysis based on filtering by the following criteria: unique molecular identifier counts per cell <200, gene count per cell >7500, and the fraction of transcripts mapped to mitochondrial genes >25% (to exclude dead or dying cells). Filtering resulted in 4,555 HFD cells at 1 mo, 4,945 control cells at 1 mo, 1,292 HFD at 3 mo, and 1,255 control cells at 3 mo, which were included in subsequent analyses. The difference in microglia counts at the 1- and 3-mo time points may have arisen to biological differences in the number of brain microglia in mice at 1 versus 3 mo,[83,84] or from technical variability, although every effort was made to mitigate contributions from this. To account for differing cell numbers at each time point, data were normalized, and ratios were reported for changes in cell type rather than changes in absolute number. Count data were then normalized using the NormalizeData function in Seurat with the default setting.

Dimension reduction, clustering, and visualization

Principal component analysis (PCA) was performed based on the top 2,000 most variable genes. The optimal principal component (PC) number was selected based on the point where the percent change in variation in consecutive PCs was lower than 0.1%. Then, Uniform Manifold Approximation and Projection (UMAP) was performed on the PCs to visualize cells, and graph-based clustering was performed on the PCA-reduced data.

Celltype annotation and differential expression analysis

To assign a cell type identity to each cluster, the cluster gene markers were identified using the FindAllMarkers function in Seurat. Cell types were assigned based on the cluster gene markers using the CellMarker[75] and PanglaoDB[74] databases and information available in the relevant literature. DESeq2[77] was used to identify differentially expressed genes (DEGs) between control and HFD cells for all microglia cell types combined and for each cell type separately. Genes were considered differentially expressed if the adjusted P-value was lower than 0.05. Kyoto Encyclopedia of Genes and Genomes (KEGG) enrichment was performed using the richR package (https://github.com/hurlab/richR) and an adjusted P-value <0.05 was chosen as the cutoff value to select significant KEGG pathways.

Cell-to-cell communication

CellChat[34] was used to examine communication among cells. CellChat uses network analysis and pattern recognition to predict major signaling inputs to cells and signaling outputs from cells. CellChat also predicts how these cells and input and output signals coordinate. First, the software identified the significant ligand-receptor pairs across cell clusters, which were classified into signaling pathways. Next, it predicted incoming signals to specific cell clusters and outgoing signals from specific cell clusters. The global communication pattern was also predicted by pattern recognition approaches. Signaling pathways were then organized by similarity measures and manifold learning from topological perspectives. Finally, CellChat calculated the communication probability of a signaling pathway by summarizing the probabilities of its associated ligand-receptor pairs.

Weighted gene co-expression network analysis

Weighted gene co-expression network analysis (WGCNA)[85] was performed to build signed co-expression networks using the WGCNA R package. The co-expression network was built using the top 3,000 most variable genes selected using the "mostVar" function from the transcripTools R package. Batch correction was done using the "ComBat" function from the sva R package. Soft power 6 was chosen by WGCNA's "pickSoftThreshold" function to calculate the adjacency matrix.

Correlation analysis of body weights to transcript levels

Correlation analysis was performed by Spearman correlation. Body weights at 1 mo and 3 mo were correlated to transcript levels at 1 mo and 3 mo in all cell clusters. Significant correlations were assessed by Spearman's rank correlation rho. Significant correlated transcripts with Benjamini-Hochberg corrected P-value<0.05 were used as input for KEGG functional enrichment analysis using richR package. The significant pathways with an adjusted P-value<0.05 were selected to generate dot plots.

Immunohistochemistry and microglial morphology analysis

One brain hemisphere from each mouse was dissected at the time of sacrifice and fixed in 4% paraformal-dehyde for ~48 h. Each brain was then placed in 10% sucrose for ~24 h, followed by 20% sucrose for ~24 h, and 30% sucrose for a minimum of 24 h. Sections (50 μm) were cut on a cryostat and immunohistochemistry was performed on floating tissue. Sections were stained with rabbit anti-Iba1 (1:1000; Wako, catalog # 019-19741) at 4°C overnight, followed by goat-anti rabbit Alexa fluor Plus 594 secondary antibody (1:2000; In-vitrogen, catalog # A32740) for 2h at room temperature followed by a Hoechst nuclear stain for 8 min. Z-stack images were acquired at 40X objective with oil immersion on a Leica Stellaris 8 Falcon Confocal Mi-croscope. Z-stacks (25.5 μm) were pre-processed using Imaris Software (Oxford Instruments). The surface rendering tool was used to identify intact microglial cells, and a mask was created and manually edited to extract the fluorescent signal of full intact cells from the raw data, while eliminating cell branches not asso-ciated with cell somas. An open microscopy environment TIF file was then run through an adapted 3DMorph script using MATLAB.[30] Objects misidentified as cells and misrepresented cells were manually removed from the final dataset. For each animal (HFD n=4, control n=3), 3 CA1 images were analyzed, and a total of 34 to 46 cells per animal were included in the final analysis.

QUANTIFICATION AND STATISTICAL ANALYSIS

Statistical analyses of mouse metabolic phenotyping was performed in Prism 9. For HFD versus control comparisons within timepoints, normality was tested using the Shapiro-Wilk test. Welch's t-test was per-formed to detect differences between groups for data with normal distributions, and the Mann-Whitney test performed for non-normally distributed data. For repeated measurements (GTTs, body mass) repeated measures 2-way ANOVA with Sidak's multiple comparisons test was performed. For microglia morphology measures, linear mixed effects models with random animal-specific intercepts were used to detect differences between diet groups. The lmerTest package in R v4.1.1 was used to fit the mixed effects models and model parameter estimates were determined using the maximum likelihood method.[86] T-tests calculated using Satterthwaite's degrees of freedom method were performed to assess differences in morphology measurements between diet groups. Histograms provided visual confirmation of assumptions of normality. The significance cutoff for all comparisons was $P<0.05$.